BioOne DIGITAL LIBRARY

Visible-Light-Driven g-C3N4/TiO2 Based Heterojunction Nanocomposites for Photocatalytic Degradation of Organic Dyes in Wastewater: A Review

Authors: Sewnet, Agidew, Abebe, Mulualem, Asaithambi, Perumal, and Alemayehu, Esayas

Visible-Light-Driven g-C$_3$N$_4$/TiO$_2$ Based Heterojunction Nanocomposites for Photocatalytic Degradation of Organic Dyes in Wastewater: A Review

Agidew Sewnet[1,2] [iD], Mulualem Abebe[1], Perumal Asaithambi[3] [iD] and Esayas Alemayehu[3,4]

[1]Faculty of Materials Science and Engineering, Jimma University, Jimma, Ethiopia, [2]Department of Physics, College of Natural and Computational Science, Bonga University, Bonga, Ethiopia, [3]Faculty of Civil and Environmental Engineering, Jimma University, Jimma, Ethiopia, and [4]Africa Center of Excellence for Water Management, Addis Ababa University, Addis Ababa, Ethiopia

ABSTRACT: Water pollution by organic contaminants is one of the most severe issues confronting the world today as a result of the rapid increase of industrialization, urbanization, human population growth, and advances in agricultural technologies. Several attempts have been made to address global water pollution issues by utilizing conventional wastewater treatment technologies. However, conventional wastewater treatment methods have several limitations such as low efficiency, high operation costs, generation of secondary waste, require additional chemicals as oxidants and extra energy. Therefore, Heterogeneous photocatalysis has gained a lot of attention in the degradation of persistent organic pollutants because it combines high efficiency, environmental friendliness, cheap cost, and safety. Subsequently, the designing of novel nanocomposite photocatalysts with strong visible light-harvesting ability, efficient charge separation and transportation, and superb stability is imminently desired for wastewater treatment. Recently, the notion of combining g-C$_3$N$_4$ with TiO$_2$ to design high photocatalytic performance heterojunction photoactive nanocomposites for organic pollutant degradation has received a lot of attention. Meanwhile, the construction of g-C$_3$N$_4$/TiO$_2$-based heterojunction nanocomposites may enhance the ability of harvesting visible light, boost charge separation and transfer efficiency, and robust photocatalytic activity. Firstly, this review concisely explained the main sources of water pollution, as well as potential treatment approaches and the fundamental mechanism of heterogeneous photocatalysis. Subsequently, the details of properties, synthesis techniques, photoactivity modification strategies, and photocatalytic applications of g-C$_3$N$_4$, TiO$_2$, and g-C$_3$N$_4$/TiO$_2$ heterojunction photocatalysts are presented. Following that, the recent advances aimed at improving the photocatalytic performance of various types of visible-light-driven g-C$_3$N$_4$/TiO$_2$ heterojunction photocatalysts for organic pollutant degradation in wastewater are presented in detail. Finally, some concluding remarks and perspectives on the challenges and opportunities for constructing different types of g-C$_3$N$_4$/TiO$_2$-based heterostructured photocatalysts are presented.

KEYWORDS: Organic contaminants, photocatalytic process, g-C$_3$N$_4$/TiO$_2$, pollutant degradation

Introduction

Nowadays, the growing global energy demand and increasing water pollution are the most serious problems presently faced worldwide due to the rampant unregulated development of industrialization, improvements in agricultural technologies, and depletion of non-renewable fossil fuels by the increase of the human population (Bustillo-Lecompte, 2015; Darkwah & Oswald, 2019; Gusain et al., 2019; Ong et al., 2016; Xu, Zhang, et al., 2018). Water is majorly polluted due to randomly discharged industrial effluents and anthropogenic activities (Gusain et al., 2019; Thines et al., 2017; Zhang, Gu, et al., 2019). Therefore, the availability of safe drinkable water free from hazardous materials, carcinogenic substances, and harmful germs has become a serious global concern (Ahmed & Haider, 2018; Manikandan et al., 2021). Moreover, the wastewater contains several types of pollutants such as organic (dyes, pesticides, pharmaceutical ingredients, fertilizers, organohalides, phenols, surfactants, etc.), inorganic (heavy metal ions, metal oxides, metal complexes, salts, etc.), nutrients, and agricultural runoff, pathogens, and so on (Gusain et al., 2019;

Thines et al., 2017; Varma et al., 2020; Zhang, Gu, et al., 2019). However, organic pollutants are responsible for major contamination of the environment due to their frequent discharge into the environment. Meanwhile, organic pollutants are prevalent in sewage effluents, groundwater, drinking water, and sludge, posing a serious hazard to people and aquatic creatures (Mahlambi et al., 2015). Therefore, organic pollutants can seriously harm the environment and cause negative effects on human health (Byrne et al., 2018; Low, Jiang, et al., 2017). Some organic pollutants are classified as persistent organic pollutants because they do not readily degrade in the environment and can persist for long periods (Mahlambi et al., 2015). Meanwhile, persistent organic pollutants were known as a kind of organic chemical contamination with high toxicity, which contaminates underground water a lot, and further leads to serious water scarcity (Xie et al., 2021). It is also suspected of causing cancer, congenital impairments, immune and reproductive system dysfunction, and endangering the growth of newborns and children (Ahmed & Haider, 2018; Gusain et al., 2019; Nadimi et al., 2019).
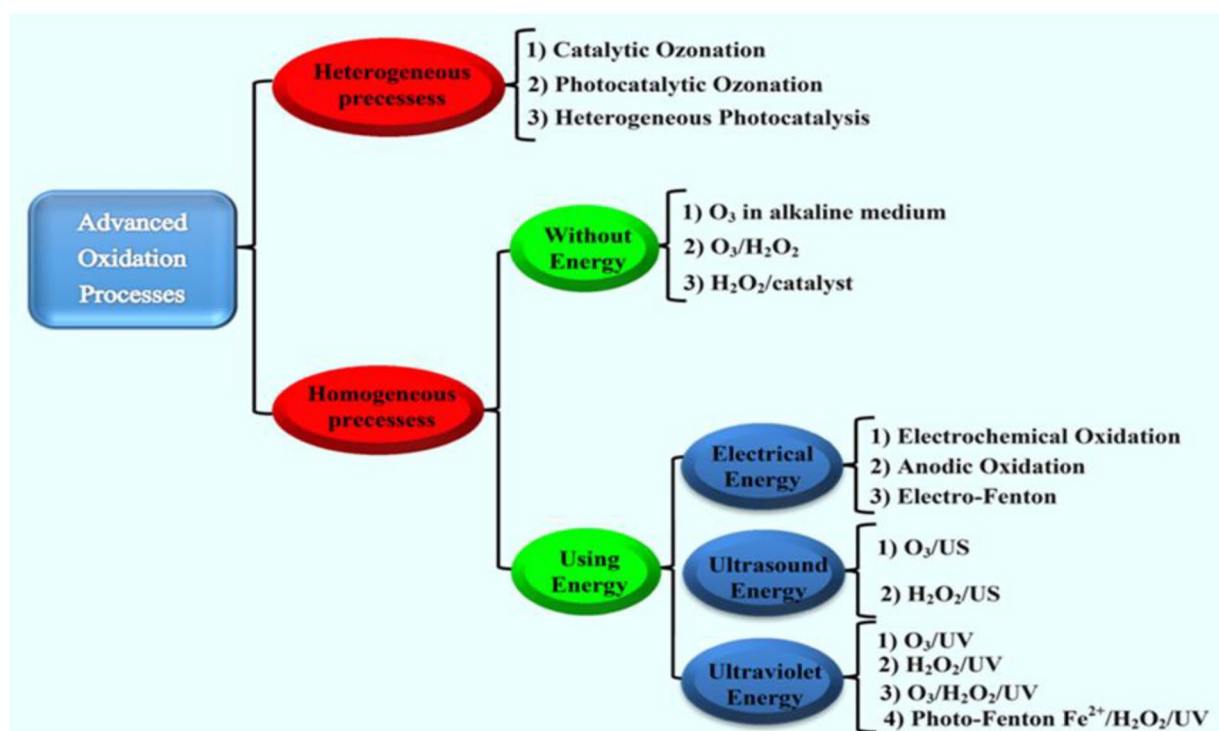
Figure 1. Various classifications of advanced oxidation process (Mousavi et al., 2018).

Among major categories of organic pollutants, modern commercial dyes are characterized by strong structural and color stability due to their high degree of aromaticity and extensively conjugated chromophores. These dyes are widely utilized in a variety of industries, including printing, leather, cosmetics, plastics, food, and, most notably, textiles, and their unintentional release into the environment poses a risk to human health and ecological systems. Furthermore, these toxic and carcinogenic synthetic colors would prevent sunlight from entering water bodies, harming natural aquatic activities including photosynthesis and other biodegradation processes. These toxins will endanger human health and the environment if they are not effectively removed (Cheng et al., 2013).

Water is the most precious resource that should be conserved, treated, and recycled scientifically for sustainable use in every aspect of life (Sudhaik et al., 2018). Therefore, various conventional approaches have been practiced for wastewater treatment such as coagulation, flocculation, filtration and membrane separation, sedimentation, reverse osmosis, adsorption, disinfection and advanced oxidation, and biological methods (Ghafoor et al., 2019; Kumar & Chowdhury, 2020; Miklos et al., 2018). However, the efficiency of these remedial techniques is limited for the purification of wastewater containing persistent organic pollutants (Iervolino et al., 2019; Sudhaik et al., 2018). Moreover, various conventional approaches are ineffective, time-consuming, chemically intensive, and have reached a significant level of maturity (Dewil et al., 2017; Kumar, Khan, et al., 2018).

For the removal of diverse contaminants from industrial wastewater, efficient wastewater treatment techniques should be utilized (Varma et al., 2020). As a result, Advanced Oxidation Processes (AOPs) are a series of chemical treatment procedures that use oxidation to mineralize organic contaminants, water pathogens, and disinfection byproducts by the in-situ production of highly reactive species (Babuponnusami & Muthukumar, 2014; Malato et al., 2009). It works by producing highly reactive chemical species such as hydroxyl radicals ($^{\bullet}OH$) and superoxide anion radicals ($^{\bullet}O_2^-$) that attack organic contaminants. The efficiency of AOPs is based on the generation of these highly reactive radicals, which are unselective and robust oxidizing species ($E^{\circ} = 2.80\,V$) capable of degrading micropollutants with reaction rate constants typically around 10^6 to 10^9 mol $L^{-1}s^{-1}$, yielding CO_2, H_2O, and, eventually, inorganic ions as final products (Ribeiro et al., 2015; Saravanan et al., 2017).

The classification of AOPs is very difficult due to the multiple processes involved. However, it can be classified as homogeneous or heterogeneous processes depending on the phase of the catalyst used (Figure 1). Despite their use in wastewater treatment, these processes have several limitations, including the need for complex equipment, ozone's short half-life, UV radiation absorption, partial mineralization of contaminants, and high costs of these processes (Sudhaik et al., 2018).

Furthermore, most AOPs require the use of additional chemicals as oxidants and energy which aggravates the energy crisis (Zhang, Gu, et al., 2019). Except for semiconductor-based Photocatalysis, the remaining advanced oxidation process have practical limitations, such as H_2O_2 transport and storage, cost-intensive oxidant synthesis, and sludge generation (Yao et al., 2014). Among the possible AOPs techniques for wastewater treatment, semiconductor-based photocatalysis has been known as a green, simple, and cost-effective technique for the complete

degradation of organic contaminants in wastewater (Gusain et al., 2020; Ismael et al., 2020). Moreover, It is by far one of the most superior and promising environmental purification technologies, not only because it uses the most plentiful solar energy and molecular oxygen (as an oxidant species), but also because it degrades persistent hazardous contaminants to carbon dioxide, water, and inorganic minerals (Dong et al., 2017; Sun et al., 2018).

The best solution for energy production and the elimination of pollutants is to use solar energy, which is a powerful, affordable, and renewable energy source (Low, Jiang, et al., 2017). Therefore, the use of sunlight is both cost-effective and environmentally friendly as well as minimizes chemicals to be used and toxic emissions in the environment for various applications (Raja & Jaffar Ali, 2021). Solar energy reaching the Earth's surface is dominated by three regions of the electromagnetic spectrum namely UV (~5%), visible (~45%), and IR (~50%) (Kumar, Karthikeyan, et al., 2018). However, the challenge here is to identify suitable photocatalytic materials capable of capturing photons, particularly those in the visible light spectrum. The search for visible light-active photocatalysts is a hot topic nowadays (Zhu et al., 2014). Therefore, the formation of heterostructured composite is desirable to utilize the extended sunlight radiation for photocatalytic applications of environmental remediation (Raja & Jaffar Ali, 2021). Moreover, constructing a heterostructured composite can greatly promote the separation of photo-generated charge carriers and the photocatalytic activity of the catalyst. The excellent photocatalytic performance of the g-C_3N_4/TiO_2 heterojunction catalysts makes them promising candidates for environmental remediation (Zhou et al., 2017). Meanwhile, g-C_3N_4 can form the heterojunction with TiO_2 to reduce the recombination of photogenerated electron-hole pairs and significantly enhance the photocatalytic activity of TiO_2 under visible light due to the close interfacial connection and appropriate conduction and valence band levels (Li et al., 2016). Due to such merits, different heterostructures of g-C_3N_4/TiO_2 nanocomposite photocatalysts have been prepared for the photodegradation of dyes in wastewater. For instance, Li et al. synthesized g-C_3N_4/TiO_2 hybrid photocatalysts through a modified sol-gel technique. Compared with pure g-C_3N_4 and TiO_2, the g-C_3N_4/TiO_2 heterojunction photocatalysts exhibited enhanced visible-light photoactivity, which is around 3.5 times as high as that of the pure g-C_3N_4 and eight times as much as the pure TiO_2. The appropriate band gap, the heterojunction between g-C_3N_4/TiO_2, and the substantially greater surface area are all factors that contribute to the high photocatalytic activity of the g-C_3N_4/TiO_2 composite. In addition, the photocatalytic performance of the g-C_3N_4/TiO_2 hybrid photocatalysts was stable, indicating that it is a promising material for dye photodegradation in wastewater (Li et al., 2016). Hao et al. fabricated g-C_3N_4/TiO_2 heterojunction composites via in situ hydrothermal synthesis followed by calcination method. Compared with pure g-C_3N_4 and TiO_2, the g-C3N_4/TiO_2 heterojunction composites exhibited higher photocatalytic

performance for decomposition of Rhodamine B (RhB), which is around 3.5 times as high as that of the pure g-C_3N_4 and 18.5 times as much as the pure TiO_2. The high activity can be ascribed to the high specific surface area of the g-C_3N_4/TiO_2 composites and a synergistic heterojunction structure between TiO_2 and g-C_3N_4 (Hao et al., 2017).

Many recent reports are not available on recent advances in g-C_3N_4/TiO_2-based nanocomposite photocatalysts for wastewater treatment. Therefore, these factors triggered the interest in this research in the near future. Herein this review will mainly focus on the recent developments and ways of boosting the photocatalytic activity of g-C_3N_4/TiO_2-based nanocomposite photocatalysts for organic pollutant degradation. Meanwhile, this critical review provides academic insight into strategies for improving charge separation and transfer efficiency, broadening visible light absorption, improving photoinduced charge carrier mobility, increasing surface area and active sites, and improving photocatalytic activity of g-C_3N_4/TiO_2-based heterostructured nanocomposites. It also pinpoints strategies for boosting the photocatalytic performance of g-C_3N_4/TiO_2-based heterojunction composites for practical application in environmental remediation. Finally, we will give a summary and outlook on constructing different types of g-C_3N_4/TiO_2-based heterostructure nanocomposite photocatalysts.

Basic Principles and Mechanism of Heterogeneous Photocatalysis

The accepted definition of photocatalysis, according to the glossary of terms and conditions used during photocatalysis, consists of a change in the rate of chemical reaction in the presence of an absorber of light by a photocatalyst in the presence of ultraviolet, visible, or infrared radiation and the photocatalyst is defined as a substance which, by absorption of ultraviolet, visible or infrared radiation, can repeatedly produce a chemical transformation of reaction partners into intermediate chemical interactions and regenerate their chemical composition after each interaction cycle (Augugliaro et al., 2019).

Among the several known advanced oxidation technologies, semiconductor-based heterogeneous photocatalysis is the most effective method for degrading contaminants without producing harmful intermediates at ambient pressure and temperature (Basavarajappa et al., 2020). In a photocatalytic process, electrons could be excited from the valence band (VB) to the conduction band (CB) of a photocatalyst, when exposed to light with energy that is greater than or equal to the bandgap energy of a photocatalyst (Sudhaik et al., 2018). Holes can directly oxidize pollutants or react with H_2O/OH^- to produce hydroxyl radicals ($^•OH$/H_2O) = 2.8 eV/NHE). Whereas the electrons capture dissolved oxygen (O_2) to yield superoxide radical (O_2/$^•O_2^-$) = –0.3 eV/NHE) (Shen et al., 2020). Moreover, the generation of $^•OH$ radicals are normally concerned with two routes, (i) H_2O and OH^- in the water environment can be readily oxidized by photogenerated h^+ to form $^•OH$ radicals; (ii) O_2 presented in the aqueous solution can be reduced by
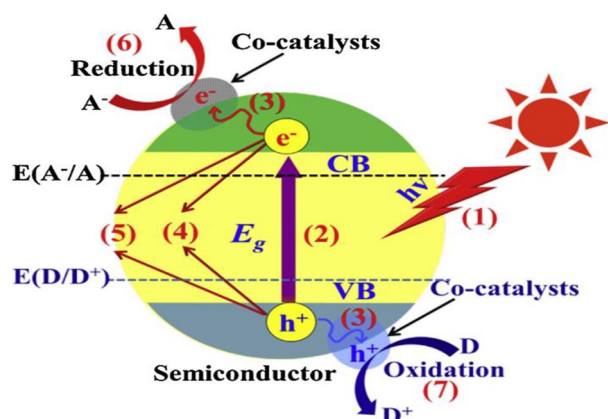
Figure 2. Schematic illustrations of major photocatalytic processes (Prasad et al., 2019).

photogenerated e^- form $\cdot O_2^-$ radicals, followed by reacting with h^+ (forming $\cdot OOH$ radicals) and further decomposition to produce $\cdot OH$ radicals (Dong et al., 2015; Huang et al., 2019; Muhd Julkapli et al., 2014). Under appropriate conditions, photocatalysis generates reactive oxygen species (ROS) like; $\cdot OH$, $\cdot O_2^-$, $^1O_2$, H_2O_2, and holes (h^+) which can facilitate the degradation of pollutants (Kumar, Raizada, et al., 2020).

Finally, Photo-generated electron-hole pairs migrate to the surface of the photocatalyst to participate in redox reactions to degrade pollutants (Sudhaik et al., 2018). Moreover, with the irradiation of UV or visible light with energy larger than or equal to the semiconductor's energy bandgap, the electron-donating, and electron-accepting sites are formed inside the surface of the semiconducting catalyst (Shen et al., 2020). However, if the photogenerated electrons and holes are not scavenged immediately after photoexcitation, they may recombine on the surface or in the bulk of the semiconductor, releasing the absorbed energy as heat or light (Huang et al., 2019; Muhd Julkapli et al., 2014).

In general, each photocatalytic reaction involves seven key steps which can be categorized into four main stages: light absorption through the semiconductor to generate pairs of electron-hole (stage 1); charge excitation (stage 2); charge separation and migration to the semiconductive surface or bulk recombination (stages 3, 4, and 5); and surface redox reactions (stages 6 and 7). These four steps are mutually exclusive, and the thermodynamics and kinetics of these processes determine the efficiency of the photocatalyst (Figure 2) (Wen et al., 2017).

Moreover, the overall photocatalyst efficiency has been significantly affected by the combined effects of four-stage processes such as (a) light absorption, (b) charge separation efficiency, (c) charge migration and transportation efficiency, and (d) charge usage efficiency. The overall efficiency of the various photocatalytic processes can be described as follows:

$$\eta_c = \eta_{abs} \times \eta_{cs} \times \eta_{cmt} \times \eta_{cu} \qquad (1)$$

Where η_c is the solar energy conversion efficiency, η_{abs} is the light absorption efficiency, η_{cs} is the charge excitation/separation efficiency, η_{cmt} is the charge migration and transportation

efficiency, and η_{cu} is the charge usage efficiency for photocatalysis reactions. Therefore, all of these typical four-step processes must be fully considered and optimized to design highly efficient visible-light-driven photocatalysts for organic pollutant degradation (Wen et al., 2015, 2017).

Structure and Photocatalytic Properties TiO$_2$ Photocatalysts

Among all semiconductor photocatalysts, TiO$_2$ is receiving tremendous attention as a promising photocatalyst for environmental remediation due to its intriguing photocatalytic properties such as higher redox potential, high reactivity, higher efficiency, robust chemical stability, non-toxicity, ease of preparation, and cost-effective (Peiris et al., 2021; Tsang et al., 2019). It exists commonly in three crystalline phases such as anatase, rutile, and brookite (Figure 3) (Jianmin & Informatio, 2016; Pelaez et al., 2012). The dominant faces in the morphology of crystalline anatase are (011) and (001). The (001) face is highly reactive and it affects the catalytic activity, stability, and absorptive properties (Peiris et al., 2021). Moreover, anatase and rutile are the most commonly used in photocatalytic applications, although anatase is considered to be more photoactive than rutile, because of its stronger reducing power and better hole-trapping ability (Gopalan et al., 2020; Tobaldi et al., 2013). Among these three polymorphs, rutile is the most stable whereas anatase and brookite are metastable phases (Singh & Dutta, 2018). Therefore, the brookite and anatase polymorphs will change into the thermodynamically stable rutile polymorph when calcined at high temperatures exceeding 600°C (Jianmin & Informatio, 2016; Pelaez et al., 2012). Brookite is generally more reactive than anatase. However, preparing pure brookite without rutile or anatase is rather difficult, and therefore it has not been widely investigated (Di Paola et al., 2013). Other than pure anatase TiO$_2$ products, some commercial TiO$_2$ products contain pure anatase or a mixture of 25% rutile and 75% anatase with a bandgap in the range of 3.15 to 3.21 eV (Tsang et al., 2019). The overlapping of 2p orbitals of oxygen forms a valance band (VB) in these crystalline phases, whereas the 3d orbitals of Ti^{4+} are responsible for the formation of the lower half of the conduction band (CB) (Daghrir et al., 2013). Anatase crystal structure comes from corner-sharing of the octahedral which forms (001) planes resulting in the tetragonal structure; whereas the rutile crystal structure comes from the edge-sharing of (001) planes of octahedral which gives a tetragonal structure (Pelaez et al., 2012). In the case of brookite, both the edge and corner-sharing provide an orthorhombic structure (Chen & Mao, 2007). The Ti-Ti distances in anatase are longer than the Ti-O distance, which results in differences in their electronic band structures (Burdett et al., 1987). Rutile has a higher density than anatase, and these structural differences result in differences in photocatalytic activity (Gupta & Tripathi, 2011; Nolan et al., 2010).
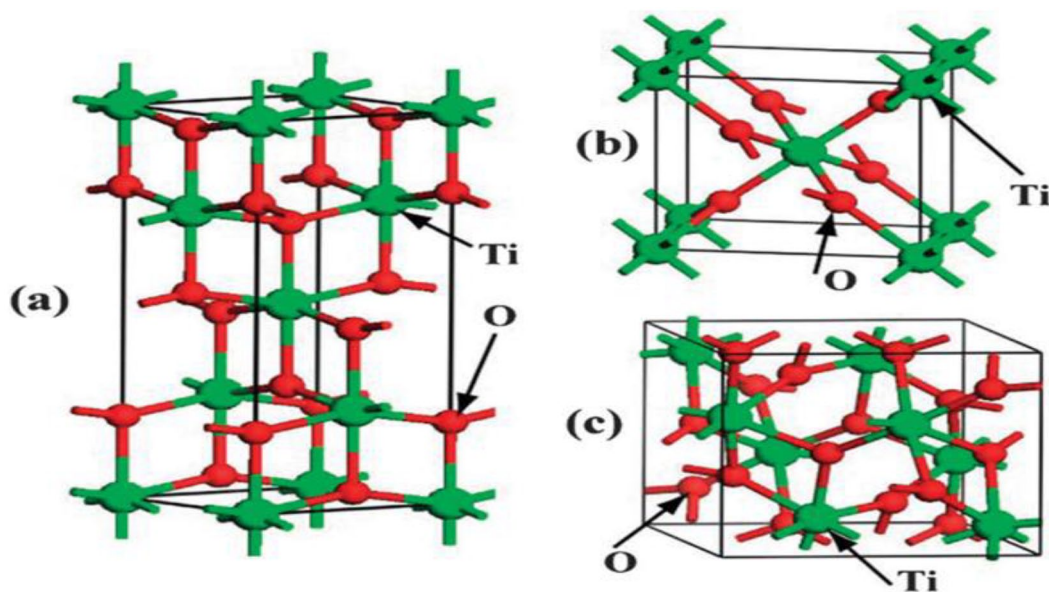
Figure 3. Crystal structure of TiO_2 polymorphs: (a) anatase, (b) rutile, and (c) brookite (Zhang et al., 2014).

Strategies for improving TiO_2 photoactivity

The modification of TiO_2 to overcome the limitations in the use of pure TiO_2 is one of the most widely studied topics in the field of photocatalysis. In recent years, some of the major approaches have been proposed to boost the photocatalytic activity of TiO_2 such as elemental doping, constructing heterojunctions with other small bandgap semiconductors, noble metal deposition, and dye sensitization (Li et al., 2020).

Doping of metal and nonmetal elements. The most significant factor that hindered the practical application of TiO_2 is the fast recombination of photoinduced electron-hole pairs and poor photosensitivity of TiO_2 under visible light irradiation. In general, ordinary TiO_2 has a wide intrinsic band gap (3.2 eV for anatase and 3.0 eV for rutile), allowing it to absorb only UV light, which accounts for just 5% of the sunlight (Li et al., 2020). Therefore, absorption of only ultraviolet radiation limits the use of all the energy of sunlight to activate photocatalytic processes (Salomatina et al., 2021). The visible light absorption of TiO_2 can be enhanced through metal and non-metal doping of the photocatalyst (Nasirian et al., 2018). Moreover, Doping causes the production of vacancies such as interstitial or substitutional defects which alter the color, conductivity, reactivity, and optical and magnetic properties of doped oxides (Rahimi et al., 2016). Enhancing the photocatalytic activity of TiO_2 by doping metals or non-metal ions has been presented in recent reviews (Basavarajappa et al., 2020; Tsang et al., 2019; Varma et al., 2020; Wen et al., 2015; Yadav & Jaiswar, 2017).

Constructing heterojunctions. The photocatalytic efficiency of TiO_2 may be significantly improved by combining it with other small bandgap semiconductors to produce a heterojunction. This approach may not only enhance the separation of photogenerated electron-hole pairs, but it can also extend the spectral response range to visible light and even the near-infrared region

(Li et al., 2020). The main design considerations of heterostructures are focused on extending light absorption, increasing specific surface area, introducing cocatalyst to reduce the overpotential of catalytic reaction, and improving the separation of photogenerated electron-hole pairs. Therefore, the design of heterojunction nanocomposites has become a compelling and feasible approach to overcoming the limitations of pristine TiO_2 in terms of photocatalytic activity (Fu et al., 2018; Low, Yu et al., 2017; Ong et al., 2016).

In particular, coupling TiO_2 with graphitic carbon nitride (g-C_3N_4) represents an intriguing solution to enhance the photocatalytic activities of TiO_2. Additionally, the delocalized conjugated structure of g-C_3N_4 gives rise to a slow charge recombination rate and promotes photoinduced charge carriers separation and transportation. In contrast, the formation of a charge-transfer complex at the interface between g-C_3N_4 and TiO_2 results in a g-C_3N_4/TiO_2 heterojunction that shows a decrease in the recombination rate of photogenerated electron-hole pairs as well as an increase in the photocatalytic activity of TiO_2 under visible light irradiation (Porcu et al., 2020; Zhou et al., 2017). There have been excellent reviews on heterojunction-based photocatalysts for the degradation of persistent organic pollutants and readers can refer to these review articles (Low, Yu, et al., 2017; Xie et al., 2021).

Various types of g-C_3N_4/TiO_2-based nanocomposite heterojunctions for organic pollutant degradation in wastewater are presented in detail in this review. Meanwhile, Tables 1 to 3 sum up the latest reports on different types of g-C_3N_4/TiO_2-based nanocomposite heterojunctions for photodegradation of organic pollutants in wastewater.

Noble-metals deposition. The deposition of a noble metal on semiconductor nanoparticles is an important factor in improving the efficiency of photocatalytic reactions. Subsequently, it

Table 1. Recent Developments on the Photocatalytic Application of g-C$_3$N$_4$/TiO$_2$-Based Type-II Heterojunction Nanocomposites for the Degradation of Organic Pollutants.

PHOTOCATALYST	SYNTHESIS METHOD	LIGHT SOURCE (CUTOFF FILTER)	POLLUTANT CONCENTRATION	REACTION TIME	DEGRADATION EFFICIENCY (%)	REFERENCE
g-C$_3$N$_4$-C/N-TiO$_2$	Thermal transformation	100W Halogen lamp (λ>400nm)	MB: 15 μM	100 minutes	93	Sridharan et al. (2013)
N-TiO$_2$/g-C3N4	Microwave assisted	300W Xe lamp (λ>400nm)	Rh B/MB: 10mg/L	60 minutes	77/69	Wang et al. (2013)
g-C$_3$N$_4$ NSs/N-TiO$_2$ NFs	Electrospinning/heat etching	Simulated solar light	Rh B: 10ppm	300 minutes	100	Han et al. (2015)
g-C$_3$N$_4$/TiO$_2$	Hydrothermal	300-W Xe lamp (λ>400nm)	MO: 100 μM	300 minutes	40	Mohini and Lakshminarasimhan (2016)
g-C$_3$N$_4$/TiO$_2$	Sol-gel	500 W Xe lamp (λ>400nm)	MB: 10 mg/L	360 minutes	90	Li et al. (2016)
g-C$_3$N$_4$-TiO$_2$-GA	Hydrothermal/freeze-drying	500 W Xe lamp (λ>400nm)	RhB: 20mg/L	60 minutes	98	Zhang et al. (2018)
C-TiO$_2$/g-C$_3$N$_4$	Hydrothermal	300W Xe lamp (λ>400nm)	MO: 20mg/L	60 minutes	99	Lu et al. (2017)
g-C$_3$N$_4$/TiO$_2$ NTs	Hydrothermal/calcination	450W Xe lamp (λ>400nm)	SMT: 5 mg/L	300 minutes	100	Ji et al. (2020)
g-C$_3$N$_4$/TiO$_2$ NTs	Chemical vapor deposition	300W Xe lamp (λ>400nm)	RhB: 5mg/L	150 minutes	99	Liu, Bie, et al. (2019)
D35-TiO$_2$/g-C$_3$N$_4$	Hydrothermal	300W Xe lamp (λ>400nm)	BPA: 10mg/L	15 minutes	100	Yang et al. (2019)
g-C$_3$N$_4$-TiO$_2$	Hydrothermal	Sunlight irradiation	BG/BPA : 20mg/L	150/240 minutes	95/88	Sutar et al. (2020)
g-C$_3$N$_4$-TiO$_2$	Hydrothermal	300W Xe lamp Without UV filter	MB: 10mg	180 minutes	80	Gündoğmuş et al. (2020),
GQDs/Mn-N-TiO2/g-C$_3$N$_4$	Hydrothermal	300W Xe lamp (320 ≤ λ ≤ 780 nm)	4-NP/CIP/DEP : 10mg/L	120 minutes	89/70/49	Nie et al. (2018)
g-C$_3$N$_4$/TiO$_2$/Kaolinite	Mild sol-gel/chemical stripping	Xe lamp (λ>400nm)	CIP: 10mg/L	240 minutes	92	Li, Sun, et al. (2018)

Note. DE = degradation efficiency; NSs = nanosheets; NTs = nanotubes; D35 = D35 dye; NFs = nanofibers; MB = methylene blue; MO = methyl orange; Rh B = rhodamine B; SMT = Sulfamethazine: BPA = bisphenol A; BG = brilliant green; CIP = ciprofloxacin; GQDs = Graphene quantum dots; GA = graphene aerogel.

Table 2. Summary of All-Solid-State Indirect Z-Scheme g-C$_3$N$_4$-TiO$_2$ Based Heterojunction Nanocomposites for Degradation of Organic Pollutants in Wastewater.

PHOTOCATALYST	SYNTHESIS METHOD	LIGHT SOURCE (CUTOFF FILTER)	POLLUTANT CONCENTRATION	REACTION TIME	DEGRADATION EFFICIENCY (%)	REFERENCE
g-C$_3$N$_4$/TiO$_2$ NTAs	Immersing/calcination	300W Xe lamp (λ ≥420nm)	Rh B: 5mg/L	5 hours	67	Zhou, Chen et al. (2016)
g-C$_3$N$_4$NSs/TiO$_2$ NTAs	Simple dispersing/anodization	300W Xe lamp (λ ≥420nm)	Rh B: 5mg/L	5 hours	76	Zhou, Chen et al. (2016)
g-C$_3$N$_4$-RGO-TiO$_2$	liquid-precipitation	300W Xe lamp (λ ≥420nm)	MB: 30mg/L	3 hours	92	Wu et al. (2017)
TiO$_2$NPs-Fe-C$_3$N$_4$ NSs	Grafting-calcination	N/A	MO:10mg/L	1 hour	89	Xu et al. (2019)
g-C$_3$N$_4$/Pd/TiO$_2$	Photo-deposition/calcination process	300W Xe lamp (λ ≥420nm)	Propylene: 0.5 mmol/L	13 minutes	34	Guo et al. (2018)
g-C$_3$N$_4$/TiO$_2$	Sol-gel/spin coating	300W Xe lamp (λ ≥420nm)	RhB/TC-HCl: 5mg/L	3 hours	31/26	Zhao et al. (2020)

Note. NTAs = nanotube arrays; NSs = nanosheets; Rh B = rhodamine B; MB = methylene blue; TC-HCl = tetracycline hydrochloride; DE = degradation efficiency.

is commonly assumed that the noble metal acts as a sink for photo-generated charge carriers and promotes interfacial charge transfer (Rahimi et al., 2016). Noble-metal nanoparticles (NPs) such as Au and Ag can respond to visible light due to the localized surface plasmon resonance (LSPR), which is the result of the collective oscillations of the surface electrons, exhibiting great potential for extending the light absorption range of wide band gap semiconductors (Lu et al., 2012). Fermi levels of these noble metals are lower than that of TiO$_2$, which results in the effective transfer of the photoinduced electrons from the conduction band of TiO$_2$ to metal particles. This electron trapping process inhibits the electron-hole recombination rate, which results in stronger photocatalytic reactions (Etacheri et al., 2015). Recently, an excellent review article has been carried out on the recent progress of noble metals with tailored features in catalytic oxidation for organic pollutants degradation (Fu et al., 2022). For instance, Moslah et al. used a sol-gel/spin-coating method for preparing nanocrystalline pure and noble metal (Ag, Au, Pd, and Pt)-doped TiO$_2$ thin films. The order of photocatalytic activity is most probably related to the work function order, Pt-TiO$_2$ > Pd-TiO$_2$ > Au-TiO$_2$ > Ag-TiO$_2$ > pure TiO$_2$ (Moslah et al., 2018).

Dye-sensitization. An intriguing strategy for achieving effective visible light-harvesting is the photosensitization of wide-band-gap semiconductors by appropriate sensitizer molecules (Dong et al., 2015). During visible-light irradiation, excited electrons are transferred from the dyes to the conduction band of the semiconductor (Etacheri et al., 2015). Meanwhile, several electron transfer steps are involved in this process. The physical adsorption of dyes occurs through the weak van der Waals interaction between the dye molecule and the TiO$_2$ surface. The photochemical process is initiated by photoexcitation of dye molecules upon irradiation by visible light, followed by the transfer of the electrons from the excited dye to the conduction band of TiO$_2$ (see Figure 4). Subsequently, in the presence of suitable electron donors (eg, EDTA, organic acids, water, alcohols, etc.), the oxidized dye is regenerated. The injection of an electron into the conduction band of TiO$_2$ is favorable due to the more negative potential of the lowest unoccupied molecular orbital (LUMO) of the dye molecules as compared to the potential of the TiO$_2$ conduction band (Daghrir et al., 2013; Rehman et al., 2009). Some dyes are even capable of producing electrons by absorbing visible light in the absence of semiconductors. Nevertheless, in the absence of semiconductor charge separators, photocatalytic activities of these dyes are too low. Visible-light absorption and electron transfer to the conduction band of TiO$_2$ often resulted in a superior photocatalytic activity (Etacheri et al., 2015). Generally, various researchers conducted a comprehensive review of different modification strategies to enhance the photocatalytic activity of TiO$_2$ (Humayun et al., 2018; Li et al., 2020; Wen et al., 2015).

Table 3. Summary of Recent Developments in Direct Z-Scheme g-C$_3$N$_4$/TiO$_2$ Heterojunction Nanocomposites for Organic Pollutant Degradation.

PHOTOCATALYST	SYNTHESIS METHOD	LIGHT SOURCE (CUTOFF FILTER)	POLLUTANT CONCENTRATION	REACTION TIME	DEGRADATION EFFICIENCY	REFERENCE
g-C$_3$N$_4$-TiO$_2$ NTs/Nps	Wetness impregnation	N/A	Isoniazid: 50 mg/L	240 minutes	91	Jo and Natarajan (2015)
g-C$_3$N$_4$/TiO$_2$-HNB	Solvothermal	3W LED UV (355 ≤ λ ≤ 375nm)	X3B: 0.1 mmol/L	45 minutes	100	Huang et al. (2015)
CN QDs- rTiO$_2$	Calcination	500W Xe lamp	RhB: 5 mg/L	300 minutes	95	Li, Lv, et al., (2017)
g-C$_3$N$_4$/TiO$_2$	Calcination	300W Xe lamp (λ ≥420nm)	Propylene	60 minutes	57	Li, Zhang, et al., (2017)
g-C$_3$N$_4$-N-TiO$_2$	Simple calcination	350W Xe lamp (λ ≥420nm)	RhB: 10μM	80 minutes	96	Lu et al. (2018)
g-C$_3$N$_4$-TiO$_2$	Solvothermal	65W visible light	RhB: 5ppm	80 minutes	97	Monga and Basu (2019)
g-C$_3$N$_4$-TiO$_2$	Hydrothermal/ion-exchange	300W Xe lamp (λ ≥420nm)	RhB: 10mg/L	30 minutes	90	Liu, Wei, et al. (2020)
O-g-C$_3$N$_4$ @Fe-TiO$_2$	Fragment coating	300W Xe lamp (λ > 380nm)	MB: 20mg/L	60 minutes	100	Wang and Liu (2019)
g-C$_3$N$_4$-TiO$_2$	Solvothermal	500W Xe lamp	RhB: 10mg/L	10 minutes	100	Zhang, Li, et al. (2019)
g-C$_3$N$_4$-TiO$_2$	Solvothermal	20W UV-Vis	Acid orange 7 : 5mg/L	12 minutes	100	Liu, Li, et al. (2020)
g-C$_3$N$_4$-TiO$_2$	Impregnation	300W Xe lamp (λ ≥420nm)	Rh B: 5 mg/L	300 minutes	45	Zhou et al. (2020)
TiO$_2$/g-C$_3$N$_4$/RGO	Electrospinning/annealing	500-W Xe lamp	RhB: 10mg/L	60 minutes	99	Hu et al. (2019)
g-C$_3$N$_4$/TiO$_2$ NTs	Anodic oxidation/calcination	250W Hg lamp (λ ≥420nm)	RhB: 15mg/L	160 minutes	96	Bi et al. (2020)
CDs/TiO2/g-C3N4	Hydrothermal	350W Xe lamp (λ ≥420nm)	ENX: 4mg/L	60 minutes	92	Su et al. (2017)
g-C3N4/TiO2 /Fe3O4@SiO2	Sol-gel	64W fluorescent lamp	Ibuprofen: 2mg/L	60 minutes	98	Kumar, Khan, et al. (2018)

Note. DE = degradation efficiency; NTs = nanotubes; NPs = nanoparticles; HNB = hollow nanobox; QDs = quantum dots; RGO = reduced graphene oxide; Rh B= rhodamine B; MB = methylene blue; X3B = Brilliant Red X-3B dye; THCL = Tetracycline hydrochloride; ENX=enrofloxacin.
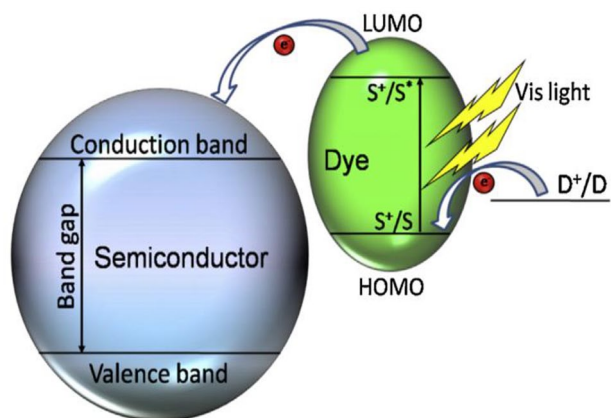
Figure 4. Mechanism of dye-sensitized semiconductor photocatalysis (Etacheri et al., 2015).

Properties, Preparation Strategies, and Photocatalytic Applications of g-C_3N_4

Origin and synthesis of g–C_3N_4

Graphitic carbon nitride (g-C_3N_4), a metal-free polymeric material containing carbon and nitrogen, the two earth-abundant elements, has exhibited excellent photocatalytic performance. Its exceptionally tunable and stable physical and chemical properties, distinctive electronic band structure along with facile synthesis makes it a unique photocatalytic material (Kumar, Raizada, et al., 2020).

Since Wang et al. first reported in 2009 on using graphitic carbon nitride as a metal-free conjugated semiconductor photocatalyst for hydrogen production, it has been regarded as a promising material for photocatalytic applications (Wang, Maeda et al., 2009). g-C_3N_4 contains seven different phases predicted by calculations of the first principle such as alpha-C_3N_4, beta-C_3N_4, pseudocubic C_3N_4, g-h-triazine, g-h-heptazine, and g-o-triazine with 5.49, 4.85, 4.30, 4.30, 2.97, 2.88, and 0.93 eV band gaps, respectively (Prasad et al., 2019; Sudhaik et al., 2018; Wen et al., 2017; Xu, Ahmed et al., 2018). A similar hardness and low compressibility to the diamond phases is the famous super hard phase β -C_3N_4 crystalline. It is also structured in the same way as Si_3N_4, replacing the silicon atom with a carbon atom. Meanwhile, because alpha-C_3N_4 is comprised of layers of beta-C_3N_4 alternating with its mirror image stack, it shares many of the same properties as beta-C_3N_4, such as crystalline structure, and bulk modulus, and atomic density (Wang et al., 2015). The remaining five phases except for the pseudocubic C_3N_4 and g-h-triazine phases have indirect band gaps in their bulk structures. With band gaps of 2.97 and 2.88 eV, the g-h-triazine and g-h heptazine phases are appropriate for a variety of visible-light active photocatalytic applications (Wen et al., 2017).

Triazine rings (C_3N_3) as tectonic units and tri-s-triazine (heptazine) ring as central units are the two fundamental building blocks of g-C_3N_4 materials. The polymer melon hypothesis is linked to tri-s-triazine, which is the most stable pattern,

energetically favored, and widely accepted structural unit (Figure 5) (Mousavi et al., 2018).

Properties and preparation of g–C_3N_4 photocatalyst

Thermogravimetric analysis shows that g-C_3N_4 is thermally stable in the air up to 600°C. It became unstable and the skeleton becomes collapsed over 600°C, and then it was completely decomposed into small CO_2 and NH_3 molecules beyond 700°C (Chen et al., 2020). Furthermore, g-C_3N_4 is chemically stable and does not dissolve in acid, alkali, or organic solvents, making it a robust material under normal conditions (Ong et al., 2016). g-C_3N_4 is not only the most stable carbon allotrope in the ambient atmosphere but also has rich surface properties which are attractive for catalysis applications due to the presence of primary surface sites (Zhu et al., 2014).

The attractive electronic structure, non-toxic, low density, earth-abundant nature, and moderate bandgap of 2.7 eV of g-C_3N_4 make it a good choice for visible light-assisted photocatalytic water purification. Furthermore, perfectly condensed g-C_3N_4 has only two earth-abundant elements: C and N, with a C/N molar ratio of 0.75, implying that g-C_3N_4 might be synthesized cheaply. Graphitic carbon nitride (g-C_3N_4) is distinguished from graphene and other analogs by its semiconductor character. Furthermore, g-C_3N_4 in nanocomposites is being investigated as a possible photocatalyst for photocatalytic organic pollutant degradation in wastewater (Sudhaik et al., 2018; Wen et al., 2017).

Pure g-C_3N_4 has a conduction band potential of around 1.3 V (normal hydrogen electrode (NHE) at pH = 7), which is more negative than the potential of photocatalytic reduction of carbon dioxide (CO_2) into hydrocarbons like methane (CH_4) (–0.24 V), methanol (CH_3OH) (–0.38 V), formaldehyde (HCHO) (–0.48 V), ethanol (CH_3CH_2OHV) (–0.33 V), and formic acid (HCOOH) (-0.61V). It's also lower than the potential for H_2 evolution, which stands at –0.41 V (NHE at pH 7). Pure g-C_3N_4 has a valence band position of +1.4 V (NHE at pH 7), which is higher than the water oxidation potential. As a result, g-C_3N_4 can be used in photocatalytic CO_2 reduction, photocatalytic water splitting, and degradation of organic pollutants (Wang et al., 2015).

Thermal polymerization, solvothermal, chemical vapor deposition, and electrochemical deposition are some of the chemical methods used to synthesize g-C_3N_4. The thermal polycondensation method, on the other hand, is universally used in a wide range of reported research due to its simple and efficient operation as well as its low cost (Tan et al., 2021). Unlike the metal-containing photocatalysts that need expensive metal salts for preparation, g-C_3N_4 is primarily produced by thermal polymerization of cheap N-rich precursors such as dicyandiamide, melamine, cyanamide, urea, and guanidine hydrochloride at various temperatures (Prasad et al., 2019; Reddy et al., 2019; Ye et al., 2015; Zhu et al., 2014). Urea was found to be a
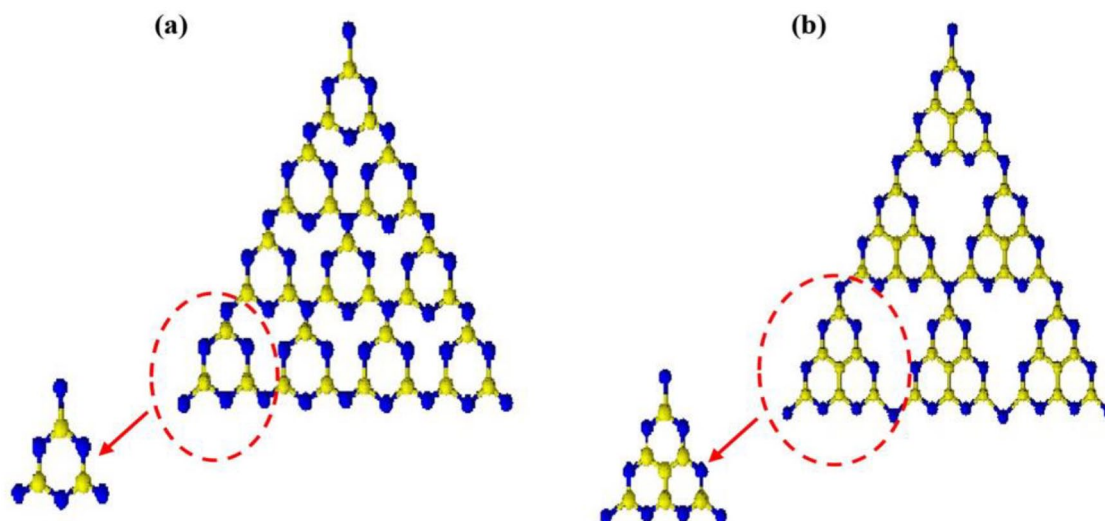
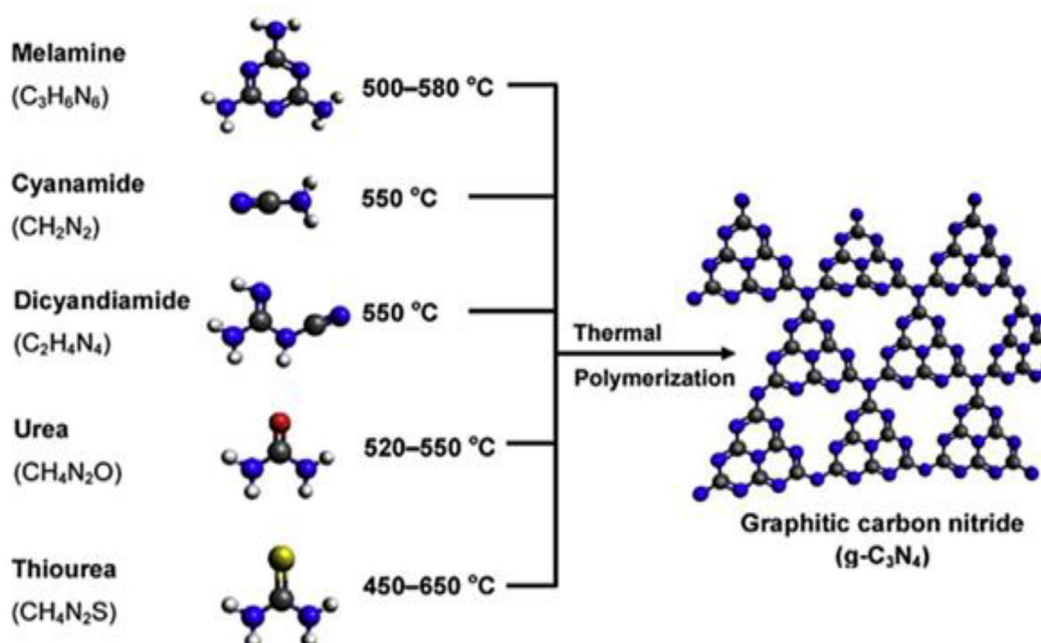**Figure 5.** s-Triazine (a and b) tri-s-Triazine (heptazine) structures of g-C$_3$N$_4$ (Mousavi et al., 2018).

Figure 6. Synthesis of graphitic carbon nitride using different precursors (Tahir et al., 2020).

superior precursor for preparing thin-layer g-C$_3$N$_4$ with a high specific surface area among the numerous precursors utilized to synthesize g-C$_3$N$_4$ (Cao et al., 2015). The temperature at which g-C$_3$N$_4$ is synthesized is determined by the type of precursor used, whereas the thickness of the g-C$_3$N$_4$ layers is determined by the pyrolysis time (Figure 6) (Tahir et al., 2020).

Modification strategies of g-C$_3$N$_4$ photoactivity

Since its discovery in 2009, scientists have worked hard to improve the photocatalytic performance of g-C$_3$N$_4$ and address its shortcomings, such as high rate of electron-hole recombination, insufficient visible light absorption ($\lambda < 460$ nm), low specific surface area (~10 m^2/g), small active sites for interfacial photoreactions, slow surface reaction kinetics, moderate oxidation ability, grain boundary effects, low charge mobility, and low quantum yield are the main disadvantages of g-C$_3$N$_4$ as photocatalyst (Sudhaik et al., 2018; Tahir et al., 2020). To improve photocatalytic activity, some major strategies have been developed, including (i) doping with metallic/non-metallic elements, (ii) coupling with other semiconductors, (iii) fabrication of mesoporous structures, and so on (Sudhaik et al., 2018).

Elemental doping of g-C$_3$N$_4$. Doping of g-C$_3$N$_4$ is a process of introducing foreign impurities into the g-C$_3$N$_4$ framework to enhance the inherent optical, electronic, luminescent, and physical properties of g-C$_3$N$_4$. In the field of photocatalysis,

band gap engineering of g-C$_3$N$_4$ via doping plays a predominant role to modulate the light absorption and redox band potentials for targeted photocatalytic applications (Ong et al., 2016).

Elemental doping is an effective strategy not only modifies the electronic band structure of g-C$_3$N$_4$ but also affects the surface properties, and improves the photocatalytic efficiency of g-C$_3$N$_4$ (Liu et al., 2021; Patnaik et al., 2021). Metal doping and nonmetal doping are the two main types of elemental doping. Metal doping endows some excellent functions to g-C$_3$N$_4$, such as reducing band gap, enhancing visible light absorption, and enhancing catalytic performance. These metals include alkali metals (Li, Na, K) and transition metals (Fe, Cu, and W), and so on (Liu et al., 2021). Metallic impurities introduce additional binding functions, lowering the bandgap and increasing visible light absorption, giving the doped system distinct catalytic and photocatalytic capabilities. To introduce metal ions into graphitic carbon nitrides, the matching soluble salt is commonly combined with the graphitic carbon nitride precursor and dissolved in deionized water while stirring to ensure uniformity (Dong et al., 2014).

Non-metal doping has proven to be an effective method to control electronic systems and improve visible light absorption (Xiao et al., 2020). Besides, Non-metal doping is a viable technique to inject heteroatoms and defects into the g-C$_3$N$_4$ matrix while keeping the metal-free characteristic. Because non-metal atoms have higher ionization energy and a different electronegativity, they can react with other substances to obtain electrons for covalent bond formation after being introduced to change the electron distribution surrounding the doped position due to charge polarization. Generally, highly electronegative doped-heteroatoms encourage electron migration from adjacent C atoms to the doping site and empower C atoms with induced polarization to demolish chemical inertia and create new reactive sites. At the same time, Lower electronegative heteroatom doping increased the asymmetric spin density of neighboring C atoms and enhanced the electron giving capacity of g-C$_3$N$_4$. These characteristics make the introduction of adsorption and activation sites and accelerate electron transfer rate. Up to now, Nonmetal heteroatoms such as C, S, and O have been highlighted in the doping modification of g-C$_3$N$_4$ (Tan et al., 2021). Recently, various excellent review articles have been carried out on improving the photocatalytic performance of g-C$_3$N$_4$ using metal and nonmetal doping (Hasija et al., 2019; Jiang et al., 2017; Liu et al., 2021; Starukh & Praus, 2020; Zhou, Zhang, et al., 2016).

Coupling with other semiconductors. The fast recombination of photoinduced electron-hole pairs causes the low efficiency of photocatalytic reactions and limited their practical photocatalytic applications. To suppress the recombination rate of photogenerated charge carriers, combining g-C$_3$N$_4$ with other semiconductors to form heterojunctions can not only improve the separation of photogenerated charge carriers but also broaden the solar light absorption spectrum (Ye et al., 2015). In general, the heterojunctions should have appropriate band positions of the two semiconductors for energy-level offsets, resulting in the accumulation of space charge at the interfaces of the two components to facilitate the separation of photogenerated carriers. Because of their excellent physical, optical, and electrical properties, g-C$_3$N$_4$-based heterojunction nanocomposites have been widely used to address a wide range of environmental pollution and energy shortages when irradiated to visible light (Huang et al., 2018). There have been comprehensive reviews on the preparation and applications of g-C$_3$N$_4$/TiO$_2$ heterojunctions to which readers can refer (Acharya & Parida, 2020; Zhou et al., 2017). Herein this review mainly focuses on different types of g-C$_3$N$_4$/TiO$_2$-based heterojunctions for photodegradation of organic pollutants, which are presented in Tables 1 to 3.

Fabrication of mesoporous structure. As a polymer, g-C$_3$N$_4$ has a flexible structure and is thus well suited to form different morphologies (Cao et al., 2015). Controlled morphologies and surface characteristics of the g-C$_3$N$_4$ nanostructure matrix are an effective technique to advance g-C$_3$N$_4$ photocatalysis with efficient charge transportation and migration as well as mass diffusion during the photocatalytic reaction (Ong et al., 2016). Indeed, several typical nanostructures of g-C$_3$N$_4$ have been obtained, such as porous g-C$_3$N$_4$, hollow spheres, and 1D nanostructures (Cao et al., 2015). Controlling the nanostructure may lead to modifications in the chemical, physical, and optical properties of g-C$_3$N$_4$. The number of redox sites, diffusion distance of electrons, and holes to reach these sites can be tuned by controlling the nanostructure (Mishra et al., 2019). Porous g-C$_3$N$_4$ photocatalysts are extremely fascinating, which can significantly increase their exposed surface area and accessible channels (porosity) and active sites in g-C$_3$N$_4$, thus facilitating the molecular mass transfer/transport, charge migration and separation, surface reactions, and light-harvesting (Cao et al., 2015; Wen et al., 2017). Moreover, g-C$_3$N$_4$ precursors like cyanamide, urea, dicyanamide, and melamine can be mixed with specific templates like silica materials, then thermally condensed. This produces a g–C$_3$N$_4$/template component, which is then removed with ammonium hydrogen fluoride or hydrofluoric acid to yield a porous g-C$_3$N$_4$ structure (Jourshabani et al., 2020; Thomas et al., 2008; Wang, Wang, & Antonietti, 2012). For instance, Shi et al. successfully synthesized spherical mesoporous g-C$_3$N$_4$ using cyanamide as a precursor and spherical mesoporous silica as a sacrificial template. The experimental results showed that as-prepared spherical g-C$_3$N$_4$ with a porous structure had a much larger surface area than bulk g-C$_3$N$_4$ for decomposing RhB under visible light, as well as excellent recycling activity (Shi et al., 2019). Similarly, Li, Huang, et al. (2018) prepared high-surface-area mesoporous
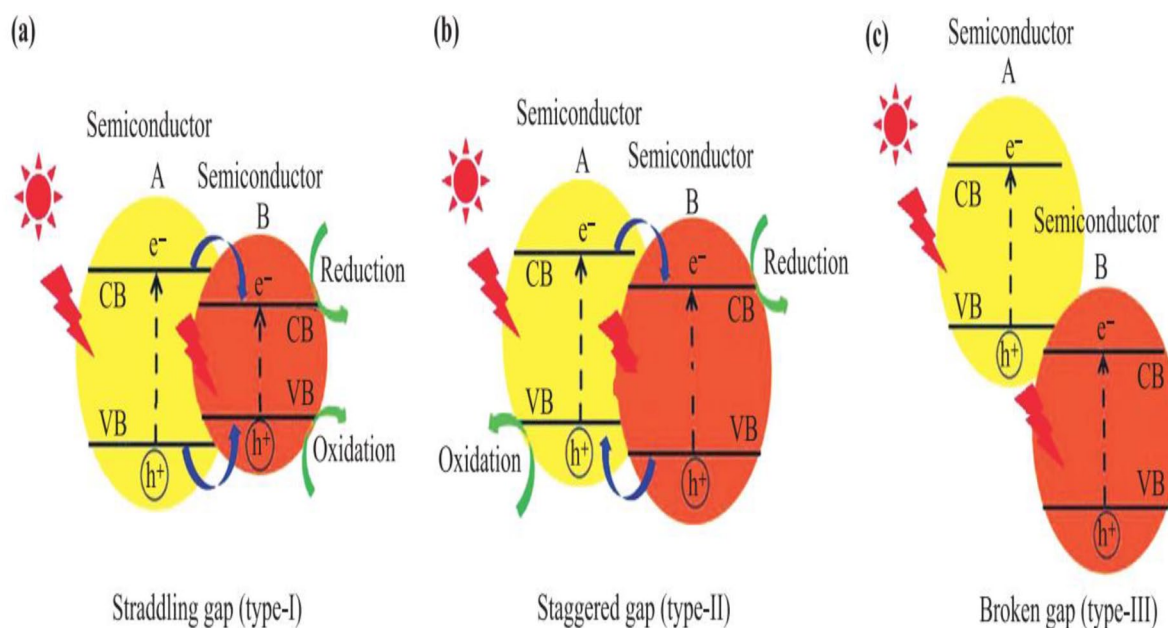
Figure 7. Schematic illustration of the mechanism of separation of electron-hole pairs in conventional heterojunction photocatalysts: (a) type-I, (b) type-II, and (c) type-III heterojunctions (Zhou et al., 2021).

g-C$_3$N$_4$ nanosheets with excellent adsorption capacity and photocatalytic activity by directly polycondensation urea followed by a one-step thermal exfoliation strategy.

Applications of g-C$_3$N$_4$/TiO$_2$ Heterojunction Nanocomposites for Photodegradation of Organic Pollutants

When g-C$_3$N$_4$ and TiO$_2$ are combined to form a g-C$_3$N$_4$/TiO$_2$ heterojunction, photocatalytic activity is significantly increased compared to single-component catalysts, making g-C$_3$N$_4$/TiO$_2$ a promising candidate for organic pollutant degradation in wastewater (Zhou et al., 2017). Due to their high activity, high thermal and chemical stability, and well-matched band structure, heterojunction catalysts made of g-C$_3$N$_4$ and TiO$_2$ have recently received a lot of attention. Various kinds of g-C$_3$N$_4$/TiO$_2$ heterojunction nanocomposite catalysts have been developed to solve water pollution problems. Meanwhile, in the case of wastewater treatment, g-C$_3$N$_4$/TiO$_2$ heterojunction nanocomposites have been widely used to degrade organic contaminants including rhodamine B (RhB), methyl orange (MO), methylene blue (MB), phenol, and so on. Summary of the recent progress on the photodegradation of organic pollutants using g-C$_3$N$_4$/TiO$_2$-based heterojunction nanocomposites are shown in Tables 1 to 3. Therefore, this review mainly focuses on type II, all-solid-state Z-scheme, and direct Z-scheme g-C$_3$N$_4$/TiO$_2$-based heterojunctions for photocatalytic decomposition of the organic contaminants from wastewater.

Conventional heterojunction photocatalytic systems

Heterojunction catalyst is one of the most popular terms in the catalytic field in recent years, and it is made up of two different band structure semiconductor catalysts that contact each other to form a catalyst heterojunction structure (Zhou et al., 2017). Heterojunction catalysts exhibit strong optical absorption ability and higher carrier utilization efficiency than single-component semiconductor catalysts. Therefore, the built-in electrostatic field of heterojunction catalyst is an effective strategy to promote the separation and transfer of photo-induced charge carriers to maximize the utilization of absorbed photons and improve photocatalytic efficiency (Wang & Liu, 2019).

As shown in Figure 7, there are typically three types of conventional heterojunction photocatalysts; straddling gap (type-I), staggered gap (type-II), and broken gap (type-III) (Low, Yu, et al., 2017; Ong et al., 2016). For type I heterojunctions, the e$^-$, and h$^+$ pairs migrate to the CB and VB of the semiconductor B, respectively. The charge carriers in the type I heterojunction photocatalyst cannot effectively separate due to their accumulation in the same semiconductor (Zhou et al., 2021).

In type-II heterojunctions, the conduction band (CB) and valance band (VB) position of semiconductor A are higher than that of the conduction band (CB) and valance band (VB) position of semiconductor B as shown in Figure 7b. Thus, the photogenerated electrons will transfer to semiconductor B, while the photogenerated holes will migrate to semiconductor A under light irradiation, resulting in a spatial separation of electron-hole pairs. Type-III photocatalyst heterojunction is similar to the type-II photocatalyst heterojunction, except that the band gaps do not overlap. As a result, electron-hole migration and separation between the two semiconductors are impossible in the type-III heterojunction, making it unsuitable for improving electron-hole pair separation (Low, Yu, et al., 2017).
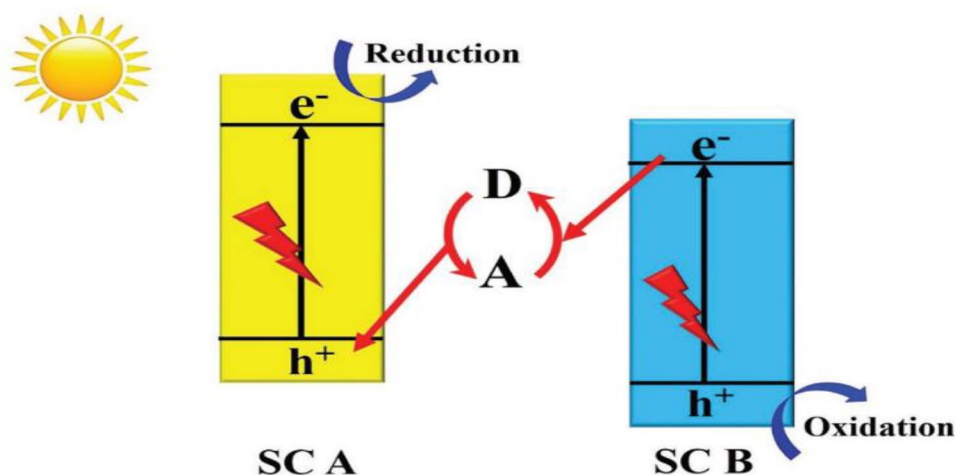
Figure 8. Schematic illustration of liquid-phase Z-scheme photocatalytic system, where A and D respectively represent the electron acceptor and donor (Low, Jiang, et al., 2017).

Because of the spatial separation of photogenerated e⁻ and h⁺ pairs, type-II heterojunction is the most successful among other types of conventional heterojunctions (Kumar, Khan, et al., 2020). The poor redox ability of type-II heterojunction photocatalysts limits their use in a wide range of applications (Low, Jiang, et al., 2017). However, recent efforts have been made to construct an efficient g-C_3N_4/TiO_2-based type-II heterojunction structure that may considerably boost the separation of photo-generated charge carriers, as well as the photocatalytic activity of the catalyst. Meanwhile, the photocatalytic performance of g-C_3N_4/TiO_2 heterojunction catalysts is good, making them suitable for the degradation of organic pollutants in wastewater (Zhou et al., 2017). In the development of type-II heterojunction, g-C_3N_4/TiO_2 composite is famous, where photo-excited electrons transferred to TiO_2 for oxidation and holes were transferred to g-C_3N_4 monolayer for a redox reaction, resulting in inhibited charge carrier recombination (Tahir et al., 2020).

Because of the excellent spatial separation of photogenerated electron-hole pairs, only type-II heterojunction is acceptable for constructing effective photocatalysts for the application of different organic pollutant degradation in wastewater, according to the aforementioned investigation (Zhou et al., 2021). Hence, a robust redox ability in type-II heterojunctions is difficult to achieve. In contrast to the traditional Type-II heterojunction, a novel type of heterojunction called a Z-scheme heterojunction has just been described to overcome this shortcoming (Ong et al., 2016).

All-solid-state indirect Z-scheme g-C_3N_4-TiO_2 heterojunction photocatalysts

In nature, It is well known that green plants can effectively convert CO_2 and H_2O to O_2 and carbohydrates through natural photosynthesis, whereby the photogenerated electrons are transported through a Z-scheme mode (Zhang et al., 2020). Furthermore, the photosynthesis of plants generally proceeds according to the so-called Z-scheme photocatalytic process, in which two isolated reactions of water oxidation and CO_2 reduction are linked together through the redox mediators (Wen et al., 2017). Typically, in a traditional Z-scheme photocatalytic system two distinct photocatalysts are linked through a suitable shuttle redox ion mediator (viz. an electron acceptor/donor (A/D) pair). The commonly used shuttle redox ion pairs are Fe^{3+}/Fe^{2+} and IO_3^-/I^-, which usually serve as electron transfer chains (Low, Jiang et al., 2017; Xu, Zhang et al., 2018).

As shown in Figure 8, both semiconductor A and semiconductor B are photoexcited when irradiated to light, resulting in the generation of electrons and holes in their respective CB and VB. The photogenerated electrons from semiconductor B will then move through a shuttle redox mediator to the VB of semiconductor A, leaving photogenerated holes in the VB of semiconductor B. As a result, the photogenerated electrons remain on semiconductor A with the greater reduction potential, while the photogenerated holes remain on semiconductor B with the higher oxidation potential, resulting in the optimization of the photocatalytic system's redox potential (Low, Jiang, et al., 2017).

However, Traditional Z-scheme photocatalysts have various limitations such as redox mediator-induced reverse reactions, in particular, is thermodynamically favorable and can readily occur because photogenerated electrons and holes with high redox power are consumed by shuttle redox ion pairs. Furthermore, the light-shielding effect, practicality constrained in solution systems, sluggish charge carrier transfer rate limited by ion-pair diffusion, and solution pH sensitivity can all contribute to traditional Z-scheme photocatalysts' limited applicability. Moreover, Most redox mediators are unstable and tend to deactivate, resulting in a reduction in reaction rate (Xu, Zhang, et al., 2018).

Tada et al. (2006) first proposed the concept of an all-solid-state Z-scheme photocatalyst, which consisted of two different semiconductors and a solid electron mediator between them.
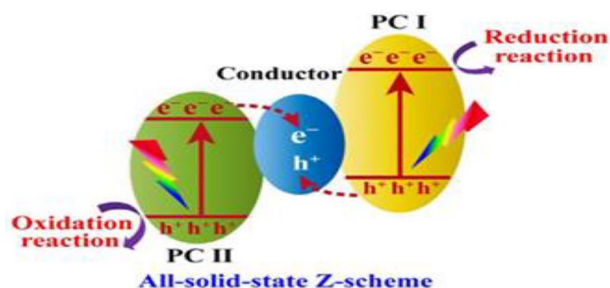
Figure 9. Schematic illustrations of charge carrier transfer mechanism in all-solid-state Z-scheme photocatalysts (Xu, Zhang, et al., 2018).

Meanwhile, For the all-solid-state Z-scheme photocatalytic system with the Ohmic-contact interfaces, their photocatalytic activities are majorly dependent on the surface properties of semiconductors with higher conduction band (CB) and valance band (VB) edges, thus leading to the robust redox ability and enhanced Photocatalytic activity. Each semiconductor in the Z-scheme photocatalytic system is responsible for one oxidation and the other for reduction reaction, thus helping for achieving the extremely extended visible-light absorption, strengthened redox ability, improved photostability, charge-separation, and photocatalytic efficiency (Wen et al., 2017).

Since the first report, Z-scheme Photocatalysis has become a promising solution for resisting environmental degradation and the global energy crisis. It works on the principle of effective separation of photogenerated electron-hole pairs and optimizes the oxidation and reduction ability of the photocatalytic system (Huang et al., 2019). Meanwhile, a Z-scheme photocatalyst may be designed based on the bandgap alignment idea to maximize photogenerated charge carrier lifetimes by suppressing charge carrier recombination for improved photocatalytic performance in the visible light spectrum (Younis & Kim, 2020).

In all-solid-state Z-scheme photocatalyst systems, the selection of a proper electron mediator is crucial because it can both efficiently transfer the photoinduced charge carriers and improve the stability of the photocatalysts. Mostly Noble metals, such as Au, Ag, and Cu NPs, have been used as excellent electron mediators for constructing all-solid-state Z-scheme photocatalysts. In addition, other carbon materials (eg, graphene, GO, RGO, CNTs) are also good candidates for electron mediators (Figure 9) (Xu, Zhang, et al., 2018).

Generally, the photocatalytic performance of Z-scheme photocatalysts is superior to that of the conventional type-II heterojunction and traditional Z-scheme photocatalytic system (Huang et al., 2019; Low, Jiang, et al., 2017). The narrower g-C_3N_4 energy bandgap (~2.7 eV) compared to TiO_2 (~3.2 eV) opens possibilities to use them in visible-light-driven photocatalysis. Furthermore, the high position of the conduction band (CB) of g-C_3N_4 enriches it with high photocatalytic reduction power and the high position of the valence band (VB) position of TiO_2 is responsible for high oxidation

power (Giannakopoulou et al., 2017). Therefore, the idea of coupling TiO_2 with g-C_3N_4 has been approved to be a promising approach to obtaining highly active photocatalysts with a visible light response and high charge carriers' separation efficiency due to their matched band structures and synergistic effects (Lu et al., 2018). Despite the attempts in structure design, conventional-type-II heterojunctions between g-C_3N_4 and TiO_2 suffer from decreasing the reduction capability of the electrons and oxidation capability of the holes after they migrate to the lower energy levels, owing to the photo-generated electrons and holes transferring to less negative and positive band sites. Therefore, to address this problem proper design of all-solid-state indirect Z-scheme photocatalytic heterojunction is significantly needed. Different from type-II heterojunction, the all-solid-state indirect Z-scheme charge transfer route could not only promote spatially charge separation, but also retain the strong redox ability of both TiO_2 and g-C_3N_4 (Liu, Zeng, et al., 2019; Lu et al., 2018).

In particular, it has been widely demonstrated that the formation of the all-solid-state Z-scheme g-C_3N_4-TiO_2 photocatalysts by different preparation methods has attracted intensive attention due to their superior photocatalytic performances. As a result, most TiO_2/g-C_3N_4 composites have been prepared by various synthesis methods including the hydrothermal method, sol-gel method, and have been widely used in many photocatalytic studies, including degradation of organic pollutants in wastewater, air purification, carbon dioxide reduction, and production of H_2 by water splitting, etc. (Lu et al., 2018).

In recent years, it has been reported that the combination of g-C_3N_4 and TiO_2 was a good candidate for the construction of the all-solid-state Z-scheme photocatalytic system. In an all-solid-state Z-scheme photocatalytic system, the photogenerated electrons prefer to remain in the conduction band (CB) of g-C_3N_4, and holes are stored in the valence band (VB) of TiO_2. Subsequently, the two oxidation and reduction processes take place simultaneously on the VB of TiO_2 and CB of g-C_3N_4, respectively. Remarkably, these two processes take place in separate places of the solid, greatly enhancing the photocatalytic efficiency (Xiao et al., 2019). This Z-scheme transfer mechanism greatly reduces the recombination rate of the electron-hole pair, thereby improving the photocatalytic activity (Bi et al., 2020). Due to the merits of the well-matched band structure of g-C_3N_4 and TiO_2, many groups have worked for years to construct effective all-solid-state Z-scheme g-C_3N_4/TiO_2 heterojunctions (Jiang et al., 2018).

In general, in the all-solid-state indirect Z-scheme g-C_3N_4-TiO_2 based photocatalysts, photo-generated electrons on TiO_2 recombine with holes on g-C_3N_4 through the electron mediators to accomplish effective separation of photo-generated electron-hole pairs with robust redox ability. Meanwhile, the particular active site and its active catalytic capability are critical to the catalytic process (Wang & Liu, 2019). In particular,
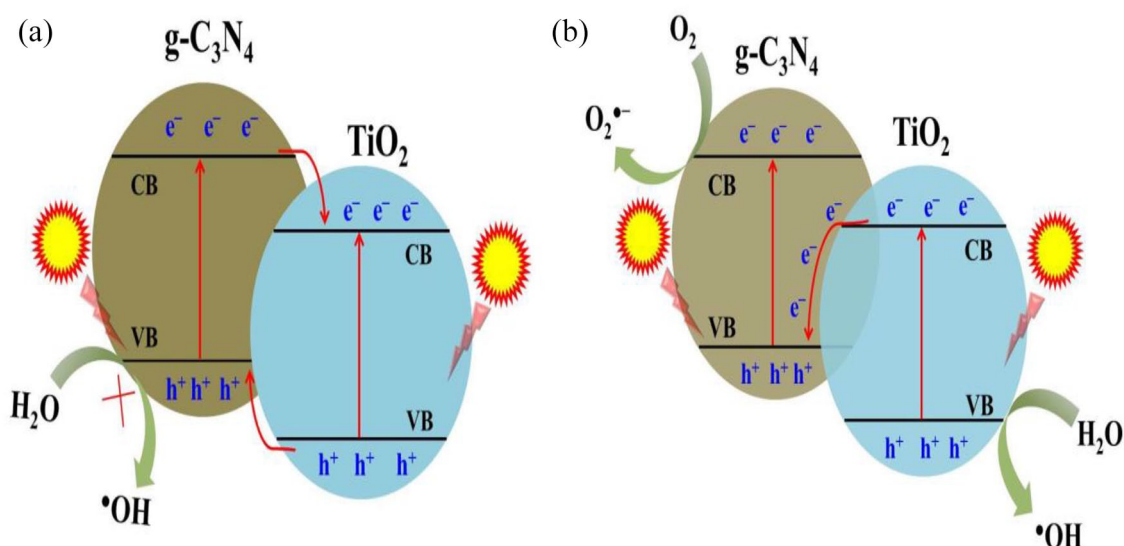
Figure 10. Schematic of electron-hole transfer mechanism of g-C_3N_4-TiO_2 type-II heterojunction (a and b) the direct Z-scheme g-C_3N_4-TiO_2 (Jo & Natarajan, 2015).

TiO_2 and g-C_3N_4 can form an all-solid-state Z-scheme heterojunction due to their matched conduction band (CB) and valence band (VB) positions, which can not only overcome the intrinsic defects of pristine photocatalyst but can also maintain the strong redox ability (Zhao et al., 2020). Moreover, coupling of narrow band-gap g-C_3N_4 with TiO_2 nanotube to construct an all-solid-state Z-scheme visible-light photocatalytic system could simultaneously possess the high charge-separation efficiency and robust redox ability under visible-light irradiation, which may produce enhanced visible-light photocatalytic activity and good stability (Zhou, Chen, et al., 2016).

Direct Z-scheme g–C_3N_4–TiO_2 heterojunction photocatalysts

A direct Z-scheme is one in which two semiconductors are joined together without the need for redox-mediators or electron mediators. The photoinduced electron-hole-pair separation method is based on the intercross-sectional electron transfer mechanism (Natarajan et al., 2018). Specifically, a typical Z-scheme system has an electron transfer process pathway that resembles the English letter "Z" hence the name Z scheme. Moreover, the band structure of a direct Z-scheme photocatalyst is similar to that of a type-II heterojunction photocatalyst (Figure 10a and b), but its charge-carrier migration mechanism is different (Huang et al., 2019). During the photocatalytic reaction, the photogenerated electrons in TiO_2 with lower reduction ability recombine with the photogenerated holes in g-C_3N_4 with a lower oxidation ability (Figure 10b) (Low, Jiang, et al., 2017). However, Due to its low potential, the hole in the valence band of g-C_3N_4 is insufficient to oxidize OH to ·OH radicals (Huang et al., 2015). Therefore, the photogenerated electrons in g-C_3N_4 with high reduction ability and photogenerated holes in TiO_2 with a high oxidation ability

can be maintained. As a result, the redox ability of the direct Z-scheme photocatalyst is significantly greater than that of the type II heterojunction photocatalyst. In addition, it should be noted that charge-carrier migration for the direct Z-scheme photocatalyst is physically more feasible than that of type-II heterojunction photocatalysts (Low, Jiang, et al., 2017).

Therefore, a direct Z-scheme can be successfully constructed if there is a suitable band structure matching between semiconductors (Tahir et al., 2020). Compared with conventional liquid phase Z-scheme and all-solid-state Z scheme photocatalytic systems, a direct Z-scheme photocatalytic system with direct contact between two components can omit the process of carriers passing through the electron mediator, greatly lowering the possibility of recombination of bulk electrons and holes. Moreover, direct Z-scheme Photocatalytic systems can reduce the cost of building photocatalytic systems, and overcome the light-shielding effect caused by the noble metal electron mediator which makes them the best candidate for water splitting, pollutant degradation, and CO_2 conversion (Huang et al., 2019). In addition, high VB and low CB are easier to generate direct Z-scheme, which has been testified to be a prospective modification for enhancing photocatalytic performance (Low, Jiang et al., 2017; Ni et al., 2021; Qi et al., 2017).

Recently, due to the relatively high cost of the commonly used electron mediators (eg, Pt, Ag, and Au), a new generation of direct Z-scheme heterojunctions without the electron mediators has attracted a great deal of attention (Low, Yu, et al., 2017). Wang, Liu, et al. (2009) constructed the first mediator-free direct Z-scheme photocatalytic system. However, Yu et al. (2013), prepared the first direct Z-scheme g-C_3N_4/TiO_2 photocatalyst without an electron mediator via a simple calcination route using inexpensive P25 and urea as feedstock, and its enhanced photocatalytic activities due to efficient separation of photo-induced charge carriers were evaluated via photocatalytic

oxidation of formaldehyde (HCHO) in the air under UV light irradiation. As a result, the transmission distance is reduced and the photocatalytic efficiency is increased (Yu et al., 2013).

In this brief review, the coupling of suitable energy band structures of g-C_3N_4 and TiO_2 to construct a direct Z-scheme photocatalytic system for photocatalytic decomposition of various organic contaminants has been explored in depth. In general, the direct Z-scheme g-C_3N_4-TiO_2 charges transfer method follows the following principles: The photo-generated electrons on TiO_2 recombine with holes on g-C_3N_4 through the built-in electrostatic field to accomplish effective separation of photo-generated electrons with higher reducibility and photo-generated holes with higher oxidizing characteristics. In the meanwhile, the particular active site and its active catalytic capability are critical to the catalytic process (Wang & Liu, 2019). Therefore, Direct Z-scheme g-C_3N_4-TiO_2 photocatalysts have numerous advantages due to their simple binary composition, high photocatalytic activity, ease of design, and ease of production. However, they have several drawbacks, including difficult control of the intimate Z-scheme interfaces with large surface area, insufficient visible-light absorption, slow reactant adsorption kinetics, and slow surface redox kinetics. Fortunately, these issues can be addressed by using an efficient electron mediator with a large surface area of earth-abundant two-dimensional conductive graphene (GR) or reduced graphene oxide (RGO) (Wu et al., 2017). Recent advances in the development of direct Z-scheme g-C_3N_4/TiO_2-based heterojunctions for photodegradation of organic pollutants are presented in Table 3.

Boosting the Photocatalytic Activity of g-C_3N_4/TiO_2-Based Nanocomposite Photocatalysts

Coupling g-C_3N_4/TiO_2 nanocomposites with graphene–based materials

The synthesis and use of carbon materials for photocatalytic applications have become a hot issue in materials research. Graphene, a unique kind of carbon material, was long considered to be thermodynamically unstable until the first experimental isolation of single-layer graphene in 2004. It has since been proved to be thermodynamically stable (Cheng et al., 2015).

Graphene has been a suitable 2D material for photocatalytic applications because of its unique properties such as ultrahigh theoretical specific surface area (2,630 m^2 g^{-1}), high chemical stability, excellent optical transmittance (97.7%), exceptional thermal conductivity (5,000 W m^{-1} K^{-1}), superior mechanical properties with Young's modulus of 1,100 GPa and high electron mobility at room temperature (200,000 cm^2 V^{-1} s^{-1}) (Chowdhury & Balasubramanian, 2014; Huang et al., 2016; Zhao et al., 2017). Meanwhile, Graphene is an excellent electron acceptor during the photocatalytic process due to its high electron mobility and extended π-π conjugation structure, which can

inhibit the recombination of photoexcited electrons and holes. Therefore, graphene is applied in photocatalysis due to its high adsorption of organic pollutants, enhanced visible light absorption, and improved separation-transportation efficiency of photogenerated charge carriers (Meng & Zhang, 2018; Zhang et al., 2017). As result, the use of graphene in the field of heterogeneous Photocatalysis provides a new dimension to enhance photocatalytic performance (Chowdhury & Balasubramanian, 2014). Graphene has a multifaceted part in enhancing the photocatalytic properties of conventional semiconductors by acting as an adsorbent, photosensitizer, photo-stabilizer, and conductor as well as co-catalyst (Sabir et al., 2021). Because of these appealing properties, combining graphene with g-C_3N_4 and TiO_2 appears to be a promising method to improve photocatalytic performance (Gusain et al., 2019; Yahya et al., 2018). Graphene can significantly improve the photoactivity of C_3N_4 by effectively separating photo-induced electron-hole pairs and significantly improving charge transfer due to the formation of a well-defined electron-hole puddle at the graphene/g-C3N4 interface (Huang et al., 2016).

For the synthesis of graphene-semiconductor-based nanocomposite photocatalysts, graphene oxide (GO) is often used as the precursor of graphene (Peiris et al., 2021). Moreover, a comprehensive review on the synthesis of graphene-based semiconductor material for photodegradation of organic pollutants is presented by Voon et al. (2016). Meanwhile, Putri et al. (2016) summarized the recent advances in the application of graphene oxide toward visible-light-driven photocatalysis. Graphene or reduced graphene oxide (rGO) can not only increase the specific surface area of the as-prepared composite but also improve its surface adsorption and reaction kinetics, resulting in a considerable increase in photocatalytic activity. The excellent electron transport capacity of reduced graphene oxide (rGO) was exploited to achieve the efficient separation of g-C_3N_4 photo-generated carriers (Hu et al., 2021; Prasad et al., 2019).

Similarly, reduced graphene oxide (rGO) is frequently used in the fabrication of heterojunction photocatalysts to increase the specific surface area and lower the recombination rate of photogenerated electron-hole pairs; as a result, photocatalytic performance is considerably improved (Hu et al., 2019). Therefore, many researchers have reported that the combination of TiO_2 and graphene-based materials (TiO_2/rGO) has intriguing photocatalytic properties such as high organic dye adsorption, suppressing photogenerated charge carrier recombination, and strong dye chromophores stacking which improves the photocatalytic activity (Huang et al., 2016). For instance, Fan et al. synthesized UV light-driven TiO_2/rGO binary nanocomposites through the sol-anaerobic calcination method for the degradation of phenol. The enhanced photocatalytic performance can be ascribed to the existence of rGO which can effectively promote the separation and transportation of photogenerated electron-hole pairs and inhibit the
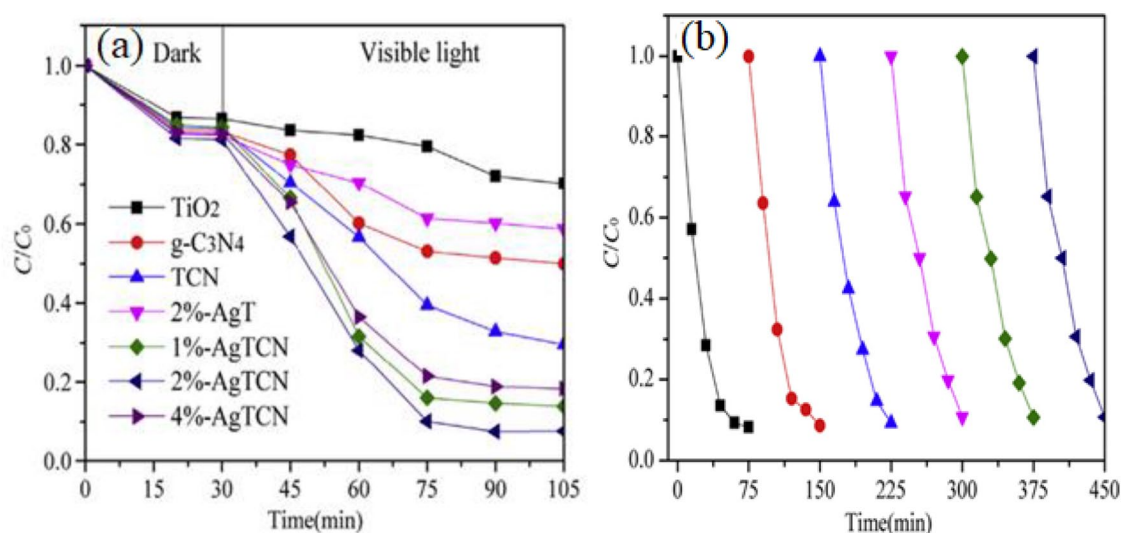
Figure 11. (a) Photocatalytic degradation of RhB under visible light irradiation and (b) recycling of the 2%-AgTCN for the removal of RhB dyes.

recombination rate of photoinduced electron-hole pairs. Moreover, TiO_2/rGO nanocomposite has a higher specific surface area and photocatalytic degradation efficiency of phenol than Pure TiO_2 (Fan et al., 2021). Subsequently, Wu et al. reported that introducing reduced graphene oxide (rGO) as an interfacial mediator into direct Z-scheme $g-C_3N_4-TiO_2$ nanocomposites can significantly improve photocatalytic activity. Meanwhile, rGO can not only act as an electron mediator to improve Z-scheme charge transportation and separation, but it can also increase the adsorption capacity of ternary composites toward the photodegradation of MB molecules. Moreover, rGO as an effective interfacial electron mediator may convert direct Z-scheme $g-C_3N_4-TiO_2$ photocatalysts to indirect Z-scheme photocatalysts with considerably improved photocatalytic efficiency, thus opening up new routes for fabricating earth-abundant ternary nanocomposite photocatalysts. Generally, diverse experimental investigations showed that rGO has multi-functional roles such as solid-state electron mediators, adsorbents, photosensitizers, and electron acceptors (Wu et al., 2017).

Constructing g–C₃N₄/TiO₂–based ternary nanocomposites by deposition of plasmonic metal nanoparticles

Nanoparticles of noble metals (Ag, Au, Pd, and Pt) can strongly absorb visible light due to their localized surface plasmon resonance (LSPR), which can be tuned by varying their size, shape, and surrounding. Furthermore, noble metal NPs can also work as electron traps and active reaction sites. These factors gave rise to a new approach to efficient visible-light photocatalysts, namely, depositing the noble metal nanoparticles on the surface of a suitable semiconductor to form a metal-semiconductor composite photocatalyst (Dhiman, 2020; Wang et al., 2012). Moreover, the strong LSPR properties of Ag and Au make them the most attractive among the other metals (Prakash et al., 2018).

For example, Chai et al. fabricated $g-C_3N_4-Pt-TiO_2$ nanocomposites via facile chemical adsorption followed by a calcination method. Meanwhile, the Pt deposited on TiO_2 surfaces in the $g-C_3N_4-TiO_2$ nanocomposite can promote the separation of photogenerated electron-hole pairs, which can effectively inhibit the recombination of photogenerated charge carriers and improve the photocatalytic activity (Chai et al., 2012). Meanwhile, Chen et al. constructed a ternary composite of $g-C_3N_4/Ag/TiO_2$ microspheres for degradation of methyl orange under visible-light irradiation. In addition, the surface plasmon resonance effect of the Ag nanoparticles exhibited enhanced visible-light absorption and photocatalytic activity of $g-C_3N_4/Ag/TiO_2$ composites than the pure TiO_2 or $g-C_3N_4$. Moreover, the $g-C_3N_4/Ag/TiO_2$ microsphere sample showed better recyclability under visible-light irradiation (Chen et al., 2014). A similar effect was also observed by Sui et al. who prepared a $g-C_3N_4/Ag/TiO_2$ (AgTCN) ternary nanocomposite catalyst by varying the loading amount of Ag nanoparticles via a simple impregnation method. The photodegradation efficiency of Rhodamine B (RhB) over 2%-AgTCN composite catalyst was 3.1 times as high as that of TiO_2 and 2.15 times $g-C_3N_4$ within 105 minutes of reaction time (as shown Figure 11). Because a Schottky barrier is formed at the interface between the Ag and TiO_2 nanoparticles, the Ag nanoparticles can serve as electron conduction bridges, which accelerates the electronic transition between the close interfaces of Ag/TiO_2 and $g-C3N4$. As a result, the electrons generated by $g-C_3N_4$ migrate to the Ag/TiO_2 surface. This process makes it easy to separate light-induced electrons and holes in space that inhibit electron-hole recombination, and boosts photocatalytic activity. In addition, the surface plasmon resonance effect of the Ag nanoparticles can promote the absorption performance of visible light. Moreover, the 2%-AgTCN composite catalyst exhibited stable photocatalytic performance with a very low activity loss after going through six cycles, which shows that it is a promising material for the degradation of organic pollutants in wastewater (Sui et al., 2020).
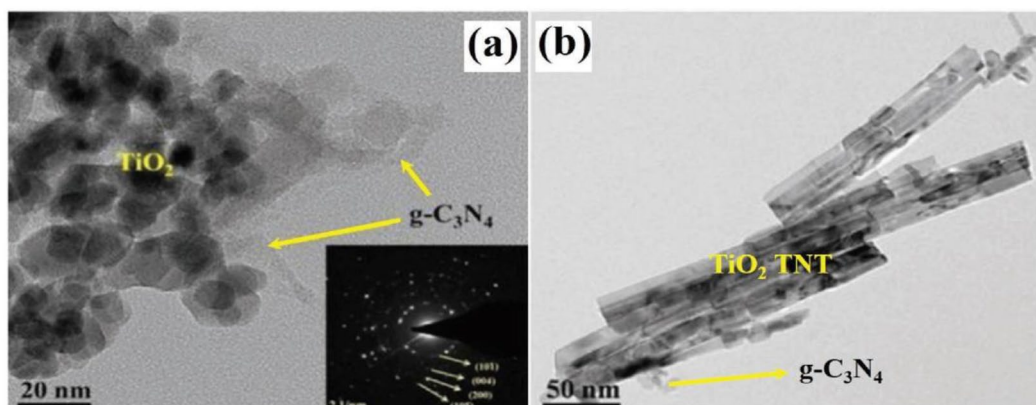
Figure 12. (a) TEM images of TiO$_2$ NPs/g-C$_3$N$_4$ and (b) TiO$_2$ nanotubes (TiO$_2$ NTs)/g-C$_3$N$_4$.

Ghafoor et al. synthesized g-C$_3$N$_4$ NS/ Ag/ TiO$_2$ NFS Z-scheme photocatalyst nanocomposites for environmental remediation for degradation of MB under simulated solar light irradiation. Moreover, the formation of Z-scheme heterojunction between TiO$_2$ and g-C$_3$N$_4$ and the surface plasmon resonance (SPR) effect of Ag nanoparticles are responsible for enhanced visible-light absorption, photocatalytic activity, and charge separation of these nanofiber composites (Ghafoor et al., 2019). Moreover, Zhang et al. synthesized Ag-TiO$_2$/rGO nanocomposite via a solvothermal method for the removal of RhB dyes. Both the adsorbent and photocatalytic activity of all the Ag-TiO$_2$/r-GO nanocomposites were much higher than pure TiO$_2$. Therefore, the large BET surface area is responsible for the superior adsorbent capacity, while the suitable structure and photocatalytic properties of graphene and the localized surface plasmon (LSPR) effect of Ag nanoparticles are responsible for the improved photocatalytic activity (Zhang et al., 2017).

Morphology controlling

It is well known that TiO$_2$ morphology has a significant influence on its photocatalytic efficiency. Consequently, researchers have made great efforts to design a g-C$_3$N$_4$/TiO$_2$ hybrid system with different TiO$_2$ morphologies such as nanoparticles, nanofibers, nanotubes, nanosheets, microspheres, and hollow nano box (Bi et al., 2020; Gündoğmuş et al., 2020; Ji et al., 2020; Jiang et al., 2017; Li, Sun, et al., 2018; Mishra et al., 2019; Sutar et al., 2020; Thomas et al., 2008; Zhou, Zhang, et al., 2016). For instance, Jo and Natarajan prepared two kinds of direct Z-scheme g-C$_3$N$_4$/TiO$_2$ (NPs and NTs) heterojunctions via a facile wetness impregnation method for the degradation of isoniazid. The photoactivity of TiO$_2$ NTs/gC$_3$N$_4$ was higher than that of TiO$_2$ NPs/gC$_3$N$_4$ because the TiO$_2$ NTs/gC$_3$N$_4$ has a larger specific surface area than TiO$_2$ NPs/gC$_3$N$_4$ to provide a greater number of surface-active sites for photocatalytic reaction. Therefore, the heterojunction built from TiO$_2$ NTs and g-C$_3$N$_4$ NSs exhibited higher photoreactivity because the high surface area and tubular structure of TiO$_2$ NTs could enhance the adsorption of pollutants and prolong the lifetime of the photogenerated charge carriers. Moreover, from this work, we can conclude that the rational tuning of the morphology of individual semiconductors is important for enhancing its photocatalytic activity (Figure 12) (Jo & Natarajan, 2015).

Conclusion and Perspectives

This review mainly focused on a comprehensive overview of the fundamental mechanisms of separation, and transportation of the photogenerated e$^-$/h$^+$ pairs of different types of g-C$_3$N$_4$/TiO$_2$ based heterostructured nanocomposite photocatalysts for environmental decontamination of organic pollutants in wastewater. Depending on the charge-carrier separation mechanism, heterojunctions can be commonly grouped into type-II, all-solid-state Z-scheme, and direct Z-scheme photocatalytic heterojunctions. Among different types of heterojunctions formed using gC$_3$N$_4$ and TiO$_2$, the redox ability of charge carriers in type-II heterojunctions decreases due to the migration of photoinduced electrons and holes to lower conduction band and valance band energy levels respectively. However, the charge transfer mechanism may improve charge carrier separation and generate photoinduced electron-hole pairs with high redox abilities and increased photocatalytic activity for both all-solid-state and direct Z-scheme photocatalysts. Moreover, gC$_3$N$_4$/TiO$_2$ heterostructured photocatalytic materials have fascinating physicochemical properties that make them potentially useful for the applications of wastewater treatment. Meanwhile, with innovative design and thorough research of their superior photocatalytic activity, the applications of g-C$_3$N$_4$/TiO$_2$-based photocatalysts for the transformation of solar to chemical energy may be significantly increased more rationally. Furthermore, the fabrication of high-performance photocatalytic systems is required to create innovative, practical, and cost-effective photocatalysts with high activity, stability, efficiency, scalability, and selectivity. Despite substantial progress in the fabrication of efficient g-C$_3$N$_4$/TiO$_2$-based heterostructured photocatalysts, photocatalytic activity remains too low for practical applications. Therefore, both experimental testing methods and theoretical material simulation using first-principles

density functional theory (DFT) might be needed to further understand the photocatalytic properties and interfacial charge separation and transfer mechanism of g-C$_3$N$_4$/TiO$_2$ hetero-structured photocatalysts. However, researchers have tried recent and practical endeavors to offer a clean environment by designing powerful photocatalytic materials using innovative synthesis techniques. Finally, Future advanced research efforts are needed to solve these issues in the near future.

Author contribution

Data Availability Statements

Declaration of Conflicting Interests

Funding

ORCID iDs

Agidew Sewnet (iD) https://orcid.org/0000-0002-2430-2690

Perumal Asaithambi (iD) https://orcid.org/0000-0002-0533-0178

REFERENCES

Acharya, R., & Parida, K. (2020). A review on TiO2/g-C3N4 visible-light- responsive photocatalysts for sustainable energy generation and environmental remediation. *Journal of Environmental Chemical Engineering*, 8, 103896. https://doi.org/10.1016/j.jece.2020.103896

Ahmed, S. N., & Haider, W. (2018). Heterogeneous photocatalysis and its potential applications in water and wastewater treatment: A review. *Nanotechnology*, 29, 342001. https://doi.org/10.1088/1361-6528/aac6ea

Augugliaro, V., Palmisano, G., Palmisano, L., & Soria, J. (2019). Heterogeneous photocatalysis and catalysis: An overview of their distinctive features. In G. Marcì & L. Palmisano (Eds.), *Heterogeneous photocatalysis: Relationships with heterogeneous catalysis and perspectives* (pp. 1–24). Elsevier. https://doi.org/10.1016/B978-0-444-64015-4.00001-8.

Babuponnusami, A., & Muthukumar, K. (2014). A review on Fenton and improvements to the Fenton process for wastewater treatment. *Journal of Environmental Chemical Engineering*, 2, 557–572. https://doi.org/10.1016/j.jece.2013.10.011

Basavarajappa, P. S., Patil, S. B., Ganganagappa, N., Reddy, K. R., Raghu, A. V., & Reddy, C. V. (2020). Recent progress in metal-doped TiO2, non-metal doped/codoped TiO2 and TiO2 nanostructured hybrids for enhanced photocatalysis. *International Journal of Hydrogen Energy*, 45, 7764–7778. https://doi.org/10.1016/j.ijhydene.2019.07.241

Bi, X., Yu, S., Liu, E., Liu, L., Zhang, K., Zang, J., & Zhao, Y. (2020). Construction of g-C3N4/TiO2 nanotube arrays Z-scheme heterojunction to improve visible light catalytic activity. *Colloids and Surfaces A Physicochemical and Engineering Aspects*, 603, 125193. https://doi.org/10.1016/j.colsurfa.2020.125193

Burdett, J. K., Hughbanks, T., Miller, G. J., Richardson, J. W., & Smith, J. V. (1987). Structural-electronic relationships in inorganic solids: Powder neutron diffraction studies of the rutile and anatase polymorphs of titanium dioxide at 15 and 295 K. *Journal of the American Chemical Society*, 109, 3639–3646. https://doi.org/10.1021/ja00246a021

Bustillo-Lecompte, C. (Ed.). (2015). *Advanced oxidation processes–Applications, trends, and prospects*. IntechOpen.

Byrne, C., Subramanian, G., & Pillai, S. C. (2018). Recent advances in photocatalysis for environmental applications. *Journal of Environmental Chemical Engineering*, 6, 3531–3555. https://doi.org/10.1016/j.jece.2017.07.080

Cao, S., Low, J., Yu, J., & Jaroniec, M. (2015). Polymeric photocatalysts based on graphitic carbon nitride. *Advanced Materials*, 27, 2150–2176. https://doi.org/10.1002/adma.201500033

Chai, B., Peng, T., Mao, J., Li, K., & Zan, L. (2012). Graphitic carbon nitride (g-C3N4)–Pt-TiO2 nanocomposite as an efficient photocatalyst for hydrogen production under visible light irradiation. *Physical Chemistry Chemical Physics*, 14, 16745–16752. https://doi.org/10.1039/c2cp42484c

Cheng, N., Tian, J., Liu, Q., Ge, C., Qusti, A. H., Asiri, A. M., Al-Youbi, A. O., & Sun, X. (2013). Au-nanoparticle-loaded graphitic carbon nitride nanosheets: Green photocatalytic synthesis and application toward the degradation of organic pollutants. *ACS Applied Materials & Interfaces*, 5, 6815–6819. https://doi.org/10.1021/am401802r

Cheng, Y., Fan, Y., Pei, Y., & Qiao, M. (2015). Graphene-supported metal/metal oxide nanohybrids: Synthesis and applications in heterogeneous catalysis. *Catalysis Science & Technology*, 5, 3903–3916. https://doi.org/10.1039/c5cy00630a

Chen, X., & Mao, S. S. (2007). Titanium dioxide nanomaterials: Synthesis, properties, modifications and applications. *ChemInform*, 38, 2891–2959. https://doi.org/10.1002/chin.200741216

Chen, Y., Huang, W., He, D., Situ, Y., & Huang, H. (2014). Construction of heterostructured g-C$_3$N$_4$/Ag/TiO$_2$ microspheres with enhanced photocatalysis performance under visible-light irradiation. *ACS Applied Materials & Interfaces*, 6, 14405–14414. https://doi.org/10.1021/am503674e

Chen, Z., Zhang, S., Liu, Y., Alharbi, N. S., Rabah, S. O., Wang, S., & Wang, X. (2020). Synthesis and fabrication of g-C3N4-based materials and their application in elimination of pollutants. *The Science of the Total Environment*, 731, 139054. https://doi.org/10.1016/j.scitotenv.2020.139054

Chowdhury, S., & Balasubramanian, R. (2014). Graphene/semiconductor nanocomposites (GSNs) for heterogeneous photocatalytic decolorization of wastewaters contaminated with synthetic dyes: A review. *Applied Catalysis B: Environmental*, 160–161, 307–324. https://doi.org/10.1016/j.apcatb.2014.05.035

Daghrir, R., Drogui, P., & Robert, D. (2013). Modified TiO2 for environmental photocatalytic applications: A review. *Industrial & Engineering Chemistry Research*, 52, 3581–3599. https://doi.org/10.1021/ie303468t

Darkwah, W. K., & Oswald, K. A. (2019). Photocatalytic applications of heterostructure graphitic carbon nitride: Pollutant degradation, hydrogen gas production (water splitting), and CO2 reduction. *Nanoscale Research Letters*, 14, 234. https://doi.org/10.1186/s11671-019-3070-3

Dewil, R., Mantzavinos, D., Poulios, I., & Rodrigo, M. A. (2017). New perspectives for advanced oxidation processes. *Journal of Environmental Management*, 195, 93–99. https://doi.org/10.1016/j.jenvman.2017.04.010

Dhiman, M. (2020). Plasmonic nanocatalysis for solar energy harvesting and sustainable chemistry. *Journal of Materials Chemistry A*, 8, 10074–10095. https://doi.org/10.1039/d0ta03114c

Di Paola, A., Bellardita, M., & Palmisano, L. (2013). Brookite, the least known TiO2 photocatalyst. *Catalysts*, 3, 36–73. https://doi.org/10.3390/catal3010036

Dong, G., Zhang, Y., Pan, Q., & Qiu, J. (2014). A fantastic graphitic carbon nitride (g-C3N4) material: Electronic structure, photocatalytic and photoelectronic properties. *Journal of Photochemistry and Photobiology C Photochemistry Reviews*, 20, 33–50. https://doi.org/10.1016/j.jphotochemrev.2014.04.002

Dong, P., Hou, G., Xi, X., Shao, R., & Dong, F. (2017). WO3-based photocatalysts: Morphology control, activity enhancement and multifunctional applications. *Environmental Science Nano*, 4, 539–557. https://doi.org/10.1039/c6en00478d

Dong, S., Feng, J., Fan, M., Pi, Y., Hu, L., Han, X., Liu, M., Sun, J., & Sun, J. (2015). Recent developments in heterogeneous photocatalytic water treatment using visible light-responsive photocatalysts: A review. *RSC Advances*, 5, 14610–14630.

Etacheri, V., Di Valentin, C., Schneider, J., Bahnemann, D., & Pillai, S. C. (2015). Visible-light activation of TiO2 photocatalysts: Advances in theory and experiments. *Journal of Photochemistry and Photobiology C Photochemistry Reviews*, 25, 1–29. https://doi.org/10.1016/j.jphotochemrev.2015.08.003

Fan, H., Yi, G., Zhang, Z., Zhang, X., Li, P., Zhang, C., Chen, L., Zhang, Y., & Sun, Q. (2021). Binary TiO2/RGO photocatalyst for enhanced degradation of phenol and its application in underground coal gasification wastewater treatment. *Optical Materials*, 120, 111482. https://doi.org/10.1016/j.optmat.2021.111482

Fu, J., Yu, J., Jiang, C., & Cheng, B. (2018). g-C3N4-based heterostructured photocatalysts. *Advanced Energy Materials*, 8, 1–31. https://doi.org/10.1002/aenm.201701503

Fu, Y., Yin, Z., Qin, L., Huang, D., Yi, H., Liu, X., Liu, S., Zhang, M., Li, B., Li, L., Wang, W., Zhou, X., Li, Y., Zeng, G., & Lai, C. (2022). Recent progress of noble metals with tailored features in catalytic oxidation for organic pollutants degradation. *Journal of Hazardous Materials*, 422, 126950. https://doi.org/10.1016/j.jhazmat.2021.126950

Ghafoor, S., Inayat, A., Aftab, F., Duran, H., Kirchhoff, K., Waseem, S., & Arshad, S. N. (2019). TiO2 nanofibers embedded with g-C3N4 nanosheets and decorated with Ag nanoparticles as Z-scheme photocatalysts for environmental remediation. *Journal of Environmental Chemical Engineering*, 7, 103452. https://doi.org/10.1016/j.jece.2019.103452

Giannakopoulou, T., Papailias, I., Todorova, N., Boukos, N., Liu, Y., Yu, J., & Trapalis, C. (2017). Tailoring the energy band gap and edges' potentials of g-C3N4/tTiOO2 composite photocatalysts for NO x removal. *Chemical Engineering Journal*, 310, 571–580. https://doi.org/10.1016/j.cej.2015.12.102

Gopalan, A. I., Lee, J. C., Saianand, G., Lee, K. P., Sonar, P., Dharmarajan, R., Hou, Y. L., Ann, K. Y., Kannan, V., & Kim, W. J. (2020). Recent progress in the abatement of hazardous pollutants using photocatalytic TiO2-based building materials. *Nanomaterials*, 10, 1854. https://doi.org/10.3390/nano10091854

Gündoğmuş, P., Park, J., & Öztürk, A. (2020). Preparation and photocatalytic activity of g-C3N4/TiO2 heterojunctions under solar light illumination. *Ceramics International*, 46, 21431–21438. https://doi.org/10.1016/j.ceramint.2020.05.241

Guo, Y., Xiao, L., Zhang, M., Li, Q., & Yang, J. (2018). An oxygen-vacancy-rich Z-scheme g-C3N4/Pd/TiO2 heterostructure for enhanced visible light photocatalytic performance. *Applications of Surface Science*, 440, 432–439. https://doi.org/10.1016/j.apsusc.2018.01.144

Gupta, S. M., & Tripathi, M. (2011). A review of TiO2 nanoparticles. *Chinese Science Bulletin*, 56, 1639–1657. https://doi.org/10.1007/s11434-011-4476-1

Gusain, R., Gupta, K., Joshi, P., & Khatri, O. P. (2019). Adsorptive removal and photocatalytic degradation of organic pollutants using metal oxides and their composites: A comprehensive review. *Advances in Colloid and Interface Science*, 272, 102009. https://doi.org/10.1016/j.cis.2019.102009

Gusain, R., Kumar, N., & Ray, S. S. (2020). Factors influencing the photocatalytic activity of photocatalysts in wastewater treatment. In: E. Fosso-Kankeu, S. Pandey, & S. S. Ray (Eds.), *Photocatalysts in advanced oxidation processes for wastewater treatment* (pp. 229–270). Wiley Online Library. https://doi.org/10.1002/9781119631422.ch8

Han, C., Wang, Y., Lei, Y., Wang, B., Wu, N., Shi, Q., & Li, Q. (2015). In situ synthesis of graphitic-C3N4 nanosheet hybridized N-doped TiO2 nanofibers for efficient photocatalytic H2 production and degradation. *Nano Research*, 8, 1199–1209. https://doi.org/10.1007/s12274-014-0600-2

Hao, R., Wang, G., Jiang, C., Tang, H., & Xu, Q. (2017). In situ hydrothermal synthesis of g-C3N4/tTioO2 heterojunction photocatalysts with high specific surface area for Rhodamine B degradation. *Applications of Surface Science*, 411, 400–410. https://doi.org/10.1016/j.apsusc.2017.03.197

Hasija, V., Raizada, P., Sudhaik, A., Sharma, K., Kumar, A., Singh, P., Jonnalagadda, S. B., & Thakur, V. K. (2019). Recent advances in noble metal free doped graphitic carbon nitride based nanohybrids for photocatalysis of organic contaminants in water: A review. *Applied Materials Today*, 15, 494–524. https://doi.org/10.1016/j.apmt.2019.04.003

Huang, D., Chen, S., Zeng, G., Gong, X., Zhou, C., Cheng, M., Xue, W., Yan, X., & Li, J. (2019). Artificial Z-scheme photocatalytic system: What have been done and where to go? *Coordination Chemistry Reviews*, 385, 44–80. https://doi.org/10.1016/j.ccr.2018.12.013

Huang, D., Yan, X., Yan, M., Zeng, G., Zhou, C., Wan, J., Cheng, M., & Xue, W. (2018). Graphitic carbon nitride-based heterojunction photoactive nanocomposites: Applications and mechanism insight. *ACS Applied Materials & Interfaces*, 10, 21035–21055. https://doi.org/10.1021/acsami.8b03620

Huang, M., Yu, J., Hu, Q., Su, W., Fan, M., Li, B., & Dong, L. (2016). Preparation and enhanced photocatalytic activity of carbon nitride / titania (001 vs 101 facets)/reduced graphene oxide (g-C 3 N 4 / TiO 2 / rGO) hybrids under visible light. *Appl. Surf. Sci*, 389, 1084–1093. https://doi.org/10.1016/j.apsusc.2016.07.180

Huang, Z., Sun, Q., Lv, K., Zhang, Z., Li, M., & Li, B. (2015). Effect of contact interface between TiO2 and g-C3N4 on the photoreactivity of g-C3N4/TiO2 photocatalyst: (0 0 1) vs (1 0 1) facets of TiO2. *Applied Catalysis B: Environmental*, 164, 420–427. https://doi.org/10.1016/j.apcatb.2014.09.043

Hu, F., Sun, S., Xu, H., Li, M., Hao, X., Shao, G., Wang, H., Chen, D., Lu, H., & Zhang, R. (2021). Investigation on g-C3N4/rgo/TiO2 nanocomposite with enhanced photocatalytic degradation performance. *Journal of Physics and Chemistry of Solids*, 156, 110181. https://doi.org/10.1016/j.jpcs.2021.110181

Hu, L., Yan, J., Wang, C., Chai, B., & Li, J. (2019). Direct electrospinning method for the construction of Z-scheme TiO2/g-C3N4/RGO ternary heterojunction photocatalysts with remarkably ameliorated photocatalytic performance. *Chinese Journal of Catalysis*, 40, 458–469. https://doi.org/10.1016/s1872-2067(18)63181-x

Humayun, M., Raziq, F., Khan, A., & Luo, W. (2018). Modification strategies of TiO$_2$ for potential applications in photocatalysis: a critical review. *Green Chemistry Letters and Reviews*, 11, 86–102. https://doi.org/10.1080/17518253.2018.1440324

Iervolino, G., Zammit, I., Vaiano, V., & Rizzo, L. (2019). Limitations and prospects for wastewater treatment by UV and visible-light-active heterogeneous photocatalysis: A critical review. *Topics in Current Chemistry*, 378, 7. https://doi.org/10.1007/s41061-019-0272-1

Ismael, A. M., El-Shazly, A. N., Gaber, S. E., Rashad, M. M., Kamel, A. H., & Hassan, S. S. M. (2020). Novel TiO2/GO/CuFe2O4 nanocomposite: A magnetic,

reusable and visible-light-driven photocatalyst for efficient photocatalytic removal of chlorinated pesticides from wastewater. *RSC Advances*, 10, 34806–34814. https://doi.org/10.1039/d0ra02874f 2020.

Jiang, G., Cao, J., Chen, M., Zhang, X., & Dong, F. (2018). Photocatalytic NO oxidation on N-doped TiO2/g-C3N4 heterojunction: Enhanced efficiency, mechanism and reaction pathway. *Applications of Surface Science*, 458, 77–85. https://doi.org/10.1016/j.apsusc.2018.07.087

Jiang, L., Yuan, X., Pan, Y., Liang, J., Zeng, G., Wu, Z., & Wang, H. (2017). Doping of graphitic carbon nitride for photocatalysis: A reveiw. *Applied Catalysis B: Environmental*, 217, 388–406. https://doi.org/10.1016/j.apcatb.2017.06.003

Jianmin, C. T. K. N., Informatio, H. L., & Yu, A. (2016). Preparation of blue TiO2 for visible-light-driven photocatalysis. In D. Yang (Ed.), *Titanium dioxide* (pp. 1–15). Intech. https://doi.org/http://dx.doi.org/10.5772/intechopen.73059.

Ji, H., Du, P., Zhao, D., Li, S., Sun, F., Duin, E. C., & Liu, W. (2020). 2D/1D graphitic carbon nitride/titanate nanotubes heterostructure for efficient photocatalysis of sulfamethazine under solar light: Catalytic "hot spots" at the rutile–anatase–titanate interfaces. *Applied Catalysis B: Environmental*, 263, 118357. https://doi.org/10.1016/j.apcatb.2019.118357

Jourshabani, M., Lee, B. K., & Shariatinia, Z. (2020). From traditional strategies to Z-scheme configuration in graphitic carbon nitride photocatalysts: Recent progress and future challenges. *Applied Catalysis B: Environmental*, 276, 119157. https://doi.org/10.1016/j.apcatb.2020.119157

Jo, W. K., & Natarajan, T. S. (2015). Influence of TiO2 morphology on the photocatalytic efficiency of direct Z-scheme g-C3N4/TiO2 photocatalysts for isoniazid degradation. *Chemical Engineering Journal*, 281, 549–565. https://doi.org/10.1016/j.cej.2015.06.120

Kumar, A., Khan, M., He, J., & Lo, I. M. C. (2020). Recent developments and challenges in practical application of visible-light-driven TiO2-based heterojunctions for PPCP degradation: A critical review. *Water Research*, 170, 115356. https://doi.org/10.1016/j.watres.2019.115356

Kumar, A., Khan, M., Zeng, X., & Lo, I. M. C.; I.M.C. Lo. (2018). Development of g-C3N4/TiO2/Fe3O4@SiO2 heterojunction via sol-gel route: A magnetically recyclable direct contact Z-scheme nanophotocatalyst for enhanced photocatalytic removal of ibuprofen from real sewage effluent under visible light. *Chemical Engineering Journal*, 353, 645–656. https://doi.org/10.1016/j.cej.2018.07.153

Kumar, A., Raizada, P., Singh, P., Saini, R. V., Saini, A. K., & Hosseini-Bandegharaei, A. (2020). Perspective and status of polymeric graphitic carbon nitride based Z-scheme photocatalytic systems for sustainable photocatalytic water purification. *Chemical Engineering Journal*, 391, 123496. https://doi.org/10.1016/j.cej.2019.123496

Kumar, K., & Chowdhury, A. (2020). *Use of novel nanostructured photocatalysts for the environmental sustainability of wastewater treatments*. Elsevier Ltd.

Kumar, S., Karthikeyan, S., & Lee, A. F. (2018). g-C3N4-based nanomaterials for visible light-driven photocatalysis. *Catalysts*, 8, 74. https://doi.org/10.3390/catal8020074

Li, C., Sun, Z., Xue, Y., Yao, G., & Zheng, S. (2016). A facile synthesis of g-C3N4/TiO2 hybrid photocatalysts by sol–gel method and its enhanced photodegradation towards methylene blue under visible light. *Advanced Powder Technology*, 27, 330–337. https://doi.org/10.1016/j.apt.2016.01.003

Li, C., Sun, Z., Zhang, W., Yu, C., & Zheng, S. (2018). Highly efficient g-C3N4/TiO2/kaolinite composite with novel three-dimensional structure and enhanced visible light responding ability towards ciprofloxacin and S. aureus. *Applied Catalysis B: Environmental*, 220, 272–282. https://doi.org/10.1016/j.apcatb.2017.08.044

Li, D.-F., Huang, W.-Q., Zou, L.-R., Pan, A., & Huang, G.-F. (2018). Mesoporous g-C$_3$N$_4$ nanosheets: Synthesis, superior adsorption capacity and photocatalytic activity. *Journal of Nanoscience and Nanotechnology*, 18, 5502–5510. https://doi.org/10.1166/jnn.2018.15441

Li, J., Zhang, M., Li, X., Li, Q., & Yang, J. (2017). Effect of the calcination temperature on the visible light photocatalytic activity of direct contact Z-scheme g-C3N4-TiO2 heterojunction. *Applied Catalysis B: Environmental*, 212, 106–114. https://doi.org/10.1016/j.apcatb.2017.04.061

Li, R., Li, T., & Zhou, Q. (2020). Impact of titanium dioxide (TiO2) modification on its application to pollution treatment—A review. *Catalysts*, 10, 804. https://doi.org/10.3390/catal10070804

Liu, M., Wei, S., Chen, W., Gao, L., Li, X., Mao, L., & Dang, H. (2020). Construction of direct Z-scheme g-C3 N 4/TiO2 nanorod composites for promoting photocatalytic activity. *Journal of the Chinese Chemical Society*, 67, 246–252. https://doi.org/10.1002/jccs.201900135

Liu, R., Bie, Y., Qiao, Y., Liu, T., & Song, Y. (2019). Design of g-C3N4/TiO2 nanotubes heterojunction for enhanced organic pollutants degradation in waste water. *Materials Letters*, 251, 126–130. https://doi.org/10.1016/j.matlet.2019.05.065

Liu, X., Li, W., Hu, R., Wei, Y., Yun, W., Nian, P., Feng, J., & Zhang, A. (2020). Synergistic degradation of acid orange 7 dye by using non-thermal plasma and g-C3N4/TiO2: Performance, degradation pathways and catalytic mechanism. *Chemosphere*, 249, 126093. https://doi.org/10.1016/j.chemosphere.2020.126093

Liu, X., Ma, R., Zhuang, L., Hu, B., Chen, J., Liu, X., & Wang, X. (2021). Recent developments of doped g-C3N4 photocatalysts for the degradation of organic

pollutants. *Critical Reviews in Environmental Science and Technology*, 51, 751–790. https://doi.org/10.1080/10643389.2020.1734433

Liu, Y., Zeng, X., Hu, X., Hu, J., Wang, Z., Yin, Y., Sun, C., & Zhang, X. (2019). Two-dimensional g-C3N4/TiO2 nanocomposites as vertical Z-scheme heterojunction for improved photocatalytic water disinfection. *Catalysis Today*, 335, 243–251. https://doi.org/10.1016/j.cattod.2018.11.053

Li, Y., Lv, K., Ho, W., Dong, F., Wu, X., & Xia, Y. (2017). Hybridization of rutile TiO2 (rTiO2) with g-C3N4 quantum dots (CN QDs): An efficient visible-light-driven Z-scheme hybridized photocatalyst. *Applied Catalysis B: Environmental*, 202, 611–619. https://doi.org/10.1016/j.apcatb.2016.09.055

Low, J., Jiang, C., Cheng, B., Wageh, S., Al-Ghamdi, A. A., & Yu, J. (2017). A review of direct Z-scheme photocatalysts. *Small Methods*, 1, 1700080. https://doi.org/10.1002/smtd.201700080

Low, J., Yu, J., Jaroniec, M., Wageh, S., & Al-Ghamdi, A. A. (2017). Heterojunction photocatalysts. *Advanced Materials*, 29(20), 1. https://doi.org/10.1002/adma.201601694

Lu, L., Wang, G., Zou, M., Wang, J., & Li, J. (2018). Effects of calcining temperature on formation of hierarchical TiO2/g-C3N4 hybrids as an effective Z-scheme heterojunction photocatalyst. *Applied Surface Science*, 441, 1012–1023. https://doi.org/10.1016/j.apsusc.2018.02.080

Lu, Y., Yu, H., Chen, S., Quan, X., & Zhao, H. (2012). Integrating plasmonic nanoparticles with TiO$_2$ photonic crystal for enhancement of visible-light-driven photocatalysis. *Environmental Science & Technology*, 46, 1724–1730. https://doi.org/10.1021/es202669y

Lu, Z., Zeng, L., Song, W., Qin, Z., Zeng, D., & Xie, C. (2017). In situ synthesis of C-TiO2/g-C3N4 heterojunction nanocomposite as highly visible light active photocatalyst originated from effective interfacial charge transfer. *Applied Catalysis B: Environmental*, 202, 489–499. https://doi.org/10.1016/j.apcatb.2016.09.052

Mahlambi, M. M., Ngila, C. J., & Mamba, B. B. (2015). Recent developments in environmental photocatalytic degradation of organic pollutants: The case of titanium dioxide nanoparticles—A review. *Journal of Nanomaterials*, 2015, 1–29. https://doi.org/10.1155/2015/790173

Malato, S., Fernández-Ibáñez, P., Maldonado, M. I., Blanco, J., & Gernjak, W. (2009). Decontamination and disinfection of water by solar photocatalysis: Recent overview and trends. *Catalysis Today 47*, 147, 1–59. https://doi.org/10.1016/j.cattod.2009.06.018

Manikandan, S., Karmegam, N., Subbaiya, R., Karthiga Devi, G., Arulvel, R., Ravindran, B., & Kumar Awasthi, M. (2021). Emerging nano-structured innovative materials as adsorbents in wastewater treatment. *Bioresource Technology*, 320, 124394. https://doi.org/10.1016/j.biortech.2020.124394

Meng, X., & Zhang, Z. (2018). Two dimensional graphitic materials for photoelectrocatalysis: A short review. *Catalysis Today*, 315, 2–8. https://doi.org/10.1016/j.cattod.2018.03.015

Miklos, D. B., Remy, C., Jekel, M., Linden, K. G., Drewes, J. E., & Hübner, U. (2018). Evaluation of advanced oxidation processes for water and wastewater treatment - A critical review. *Water Research*, 139, 118–131. https://doi.org/10.1016/j.watres.2018.03.042

Mishra, A., Mehta, A., Basu, S., Shetti, N. P., Reddy, K. R., & Aminabhavi, T. M. (2019). Graphitic carbon nitride (g–C3N4)–based metal-free photocatalysts for water splitting: A review. *Carbon*, 149, 693–721. https://doi.org/10.1016/j.carbon.2019.04.104

Mohini, R., & Lakshminarasimhan, N. (2016). Coupled semiconductor nanocomposite g-C3N4/TiO2 with enhanced visible light photocatalytic activity. *Materials Research Bulletin*, 76, 370–375. https://doi.org/10.1016/j.materresbull.2015.12.034

Monga, D., & Basu, S. (2019). Enhanced photocatalytic degradation of industrial dye by g-C3N4/TiO2 nanocomposite: Role of shape of TiO2. *Advanced Powder Technology*, 30, 1089–1098. https://doi.org/10.1016/j.apt.2019.03.004

Moslah, C., Kandyla, M., Mousdis, G. A., Petropoulou, G., & Ksibi, M. (2018). Photocatalytic properties of titanium dioxide thin films doped with noble metals (Ag, Au, Pd, and Pt). *Phys. Status Solidi Appl. Mater. Sci*, 215, 1–7. https://doi.org/10.1002/pssa.201800023

Mousavi, M., Habibi-Yangjeh, A., & Pouran, S. R. (2018). Review on magnetically separable graphitic carbon nitride-based nanocomposites as promising visible-light-driven photocatalysts. *Journal of Materials Science Materials in Electronics*, 29, 1719–1747. https://doi.org/10.1007/s10854-017-8166-x

Muhd Julkapli, N., Bagheri, S., & Bee Abd Hamid, S. (2014). Recent advances in heterogeneous photocatalytic decolorization of synthetic dyes. *Science World Journal*, 2014, 1–25. https://doi.org/10.1155/2014/692307

Nadimi, M., Ziarati Saravani, A., Aroon, M. A., & Ebrahimian Pirbazari, A. (2019). Photodegradation of methylene blue by a ternary magnetic TiO2/Fe3O4/graphene oxide nanocomposite under visible light. *Materials Chemistry and Physics*, 225, 464–474. https://doi.org/10.1016/j.matchemphys.2018.11.029

Nasirian, M., Lin, Y. P., Bustillo-Lecompte, C. F., & Mehrvar, M. (2018). Enhancement of photocatalytic activity of titanium dioxide using non-metal doping methods under visible light: A review. *International Journal of Environmental Science and Technology*, 15, 2009–2032. https://doi.org/10.1007/s13762-017-1618-2

Natarajan, T. S., Thampi, K. R., & Tayade, R. J. (2018). Visible light driven redox-mediator-free dual semiconductor photocatalytic systems for pollutant degradation and the ambiguity in applying Z-scheme concept. *Applied Catalysis B: Environmental*, 227, 296–311. https://doi.org/10.1016/j.apcatb.2018.01.015

Nie, Y. C., Yu, F., Wang, L. C., Xing, Q. J., Liu, X., Pei, Y., Zou, J. P., Dai, W. L., Li, Y., & Suib, S. L. (2018). Photocatalytic degradation of organic pollutants coupled with simultaneous photocatalytic H2 evolution over graphene quantum dots/Mn-N-TiO2/g-C3N4 composite catalysts: Performance and mechanism. *Applied Catalysis B: Environmental*, 227, 312–321. https://doi.org/10.1016/j.apcatb.2018.01.033

Ni, J., Wang, W., Liu, D., Zhu, Q., Jia, J., Tian, J., Li, Z., Wang, X., & Xing, Z. (2021). Oxygen vacancy-mediated sandwich-structural TiO2-x /ultrathin g-C3N4/TiO2-x direct Z-scheme heterojunction visible-light-driven photocatalyst for efficient removal of high toxic tetracycline antibiotics. *Journal of Hazardous Materials*, 408, 124432. https://doi.org/10.1016/j.jhazmat.2020.124432

Nolan, N. T., Seery, M. K., Hinder, S. J., Healy, L. F., & Pillai, S. C. (2010). A systematic study of the effect of silver on the chelation of formic acid to a titanium precursor and the resulting effect on the anatase to rutile transformation of TiO2. *Journal of Physical Chemistry C*, 114, 13026–13034. https://doi.org/10.1021/jp1016054

Ong, W. J., Tan, L. L., Ng, Y. H., Yong, S. T., & Chai, S. P. (2016). Graphitic carbon nitride (g-C3N4)-based photocatalysts for artificial photosynthesis and environmental remediation: Are we a step closer to achieving sustainability? *Chemical Reviews*, 116, 7159–7329. https://doi.org/10.1021/acs.chemrev.6b00075

Patnaik, S., Sahoo, D. P., & Parida, K. (2021). Recent advances in anion doped g-C3N4 photocatalysts: A review. *Carbon*, 172, 682–711. https://doi.org/10.1016/j.carbon.2020.10.073

Peiris, S., Silva, H. B., Ranasinghe, K. N., Bandara, S. V., & Perera, I. R. (2021). Recent development and future prospects of TiO2 photocatalysis. *Journal of the Chinese Chemical Society*, 68, 738–769. https://doi.org/10.1002/jccs.202000465

Pelaez, M., Nolan, N. T., Pillai, S. C., Seery, M. K., Falaras, P., Kontos, A. G., Dunlop, P. S. M., Hamilton, J. W. J., Byrne, J. A., O'Shea, K., Entezari, M. H., & Dionysiou, D. D. (2012). A review on the visible light active titanium dioxide photocatalysts for environmental applications. *Applied Catalysis B: Environmental*, 125, 331–349. https://doi.org/10.1016/j.apcatb.2012.05.036

Porcu, S., Castellino, M., Roppolo, I., Carbonaro, C. M., Palmas, S., Mais, L., Casula, M. F., Neretina, S., Hughes, R. A., Secci, F., & Ricci, P. C. (2020). Highly efficient visible light phenyl modified carbon nitride/TiO2 photocatalyst for environmental applications. *Applications of Surface Science*, 531, 147394. https://doi.org/10.1016/j.apsusc.2020.147394

Prakash, J., Sun, S., Swart, H. C., & Gupta, R. K. (2018). Noble metals-TiO2 nanocomposites: From fundamental mechanisms to photocatalysis, surface enhanced Raman scattering and antibacterial applications. *Applied Materials Today*, 11, 82–135. https://doi.org/10.1016/j.apmt.2018.02.002

Prasad, C., Tang, H., & Bahadur, I. (2019). Graphitic carbon nitride based ternary nanocomposites: From synthesis to their applications in photocatalysis: A recent review. *Journal of Molecular Liquids*, 281, 634–654. https://doi.org/10.1016/j.molliq.2019.02.068

Putri, L. K., Tan, L. L., Ong, W. J., Chang, W. S., & Chai, S. P. (2016). Graphene oxide: Exploiting its unique properties toward visible-light-driven photocatalysis. *Applied Materials Today*, 4, 9–16. https://doi.org/10.1016/j.apmt.2016.04.001

Qi, K., Cheng, B., Yu, J., & Ho, W. (2017). A review on TiO 2 -based Z-scheme photocatalysts. *Chinese Journal of Catalysis*, 38, 1936–1955. https://doi.org/10.1016/s1872-2067(17)62962-0

Rahimi, N., Pax, R. A., & Gray, E. M. (2016). Review of functional titanium oxides. I: TiO2 and its modifications. *Progress in Solid State Chemistry*, 44, 86–105. https://doi.org/10.1016/j.progsolidstchem.2016.07.002

Raja, V., & Jaffar Ali, B. M. (2021). Synergy of photon up-conversion and Z-scheme mechanism in graphitic carbon nitride nanoparticles decorated g-C3N4-TiO2. *Colloids and Surfaces A: Physicochemical and Engineering Aspects*, 611, 125862. https://doi.org/10.1016/j.colsurfa.2020.125862

Reddy, K. R., Reddy, C. V., Nadagouda, M. N., Shetti, N. P., Jaesool, S., & Aminabhavi, T. M. (2019). Polymeric graphitic carbon nitride (g-C3N4)-based semiconducting nanostructured materials: Synthesis methods, properties and photocatalytic applications. *Journal of Environmental Management*, 238, 25–40. https://doi.org/10.1016/j.jenvman.2019.02.075

Rehman, S., Ullah, R., Butt, A. M., & Gohar, N. D. (2009). Strategies of making TiO2 and ZnO visible light active. *Journal of Hazardous Materials*, 170, 560–569. https://doi.org/10.1016/j.jhazmat.2009.05.064

Ribeiro, A. R., Nunes, O. C., Pereira, M. F., & Silva, A. M. (2015). An overview on the advanced oxidation processes applied for the treatment of water pollutants defined in the recently launched Directive 2013/39/EU. *Environment International*, 75, 33–51. https://doi.org/10.1016/j.envint.2014.10.027

Sabir, R., Waheed, A., Moazzam Ali, M., & Mushtaq, U. (2021). Graphene-based photocatalysts for organic pollutant removal from waste-water: recent progress and future challenges. *Environmental Technology Reviews*, 10, 323–341. https://doi.org/10.1080/21622515.2021.1994658

Salomatina, E. V., Fukina, D. G., Koryagin, A. V., Titaev, D. N., Suleimanov, E. V., & Smirnova, L. A. (2021). Preparation and photocatalytic properties of titanium dioxide modified with gold or silver nanoparticles. *Journal of Environmental Chemical Engineering*, 9, 106078. https://doi.org/10.1016/j.jece.2021.1060782021.

Saravanan, R., Gracia, F., & Stephen, A. (2017). Basic principles, mechanism, and challenges of photocatalysis. In: M. Khan, D. Pradhan, & Y. Sohn (Eds.), *Nanocomposites for visible light-induced photocatalysis. Springer series on polymer and composite materials* (pp. 19–40). Springer. https://doi.org/10.1007/978-3-319-62446-4

Shen, Y., Dos Santos-Garcia, A. J., & Martín de Vidales, M. J. (2020). Graphitic carbon nitride-based composite in advanced oxidation processes for aqueous organic pollutants removal: A review. *Processes*, 9(1), 66. https://doi.org/10.3390/pr9010066

Shi, L., Wang, F., & Sun, J. (2019). The preparation of spherical mesoporous g-C3N4 with highly improved photocatalytic performance for H2 production and rhodamine B degradation. *Materials Research Bulletin*, 113, 115–121. https://doi.org/10.1016/j.materresbull.2019.01.028

Singh, R., & Dutta, S. (2018). Synthesis and characterization of solar photoactive TiO 2 nanoparticles with enhanced structural and optical properties. *Advanced Powder Technology*, 29, 211–219. https://doi.org/10.1016/j.apt.2017.11.005

Sridharan, K., Jang, E., & Park, T. J. (2013). Novel visible light active graphitic C3N4–TiO2 composite photocatalyst: Synergistic synthesis, growth and photocatalytic treatment of hazardous pollutants. *Applied Catalysis B: Environmental*, 142-143, 718–728. https://doi.org/10.1016/j.apcatb.2013.05.077

Starukh, H., & Praus, P. (2020). Doping of graphitic carbon nitride with non-metal elements and its applications in photocatalysis. *Catalysts*, 10, 1119. https://doi.org/10.3390/catal10101119

Sudhaik, A., Raizada, P., Shandilya, P., Jeong, D. Y., Lim, J. H., & Singh, P. (2018). Review on fabrication of graphitic carbon nitride based efficient nanocomposites for photodegradation of aqueous phase organic pollutants. *Journal of Industrial and Engineering Chemistry*, 67, 28–51. https://doi.org/10.1016/j.jiec.2018.07.007

Sui, G., Li, J., Du, L., Zhuang, Y., Zhang, Y., Zou, Y., & Li, B. (2020). Preparation and characterization of g-C3N4/Ag–TiO2 ternary hollowsphere nanoheterojunction catalyst with high visible light photocatalytic performance. *Journal of Alloys and Compounds*, 823, 153851. https://doi.org/10.1016/j.jallcom.2020.153851

Sun, Z., Wang, H., Wu, Z., & Wang, L. (2018). g-C3N4 based composite photocatalysts for photocatalytic CO2 reduction. *Catalysis Today*, 300, 160–172. https://doi.org/10.1016/j.cattod.2017.05.033

Sutar, R. S., Barkul, R. P., Delekar, S. D., & Patil, M. K. (2020). Sunlight assisted photocatalytic degradation of organic pollutants using g-C3N4-TiO2 nanocomposites. *Arabian Journal of Chemistry*, 13, 4966–4977. https://doi.org/10.1016/j.arabjc.2020.01.019

Su, Y., Chen, P., Wang, F., Zhang, Q., Chen, T., Wang, Y., Yao, K., Lv, W., & Liu, G. (2017). Decoration of TiO2/g-C3N4 Z-scheme by carbon dots as a novel photocatalyst with improved visible-light photocatalytic performance for the degradation of enrofloxacin. *RSC Advances*, 7, 34096–34103. https://doi.org/10.1039/c7ra05485h

Tada, H., Mitsui, T., Kiyonaga, T., Akita, T., & Tanaka, K. (2006). All-solid-state Z-scheme in CdS-Au-TiO2 three-component nanojunction system. *Nature Materials*, 5, 782–786. https://doi.org/10.1038/nmat1734

Tahir, M., Tasleem, S., & Tahir, B. (2020). Recent development in band engineering of binary semiconductor materials for solar driven photocatalytic hydrogen production. *International Journal of Hydrogen Energy*, 45, 15985–16038. https://doi.org/10.1016/j.ijhydene.2020.04.071

Tan, J., Li, Z., Li, J., Wu, J., Yao, X., & Zhang, T. (2021). Graphitic carbon nitride-based materials in activating persulfate for aqueous organic pollutants degradation: A review on materials design and mechanisms. *Chemosphere*, 262, 127675. https://doi.org/10.1016/j.chemosphere.2020.127675

Thines, R. K., Mubarak, N. M., Nizamuddin, S., Sahu, J. N., Abdullah, E. C., & Ganesan, P. (2017). Application potential of carbon nanomaterials in water and wastewater treatment: A review. *Journal of the Taiwan Institute of Chemical Engineers*, 72, 116–133. https://doi.org/10.1016/j.jtice.2017.01.018

Thomas, A., Fischer, A., Goettmann, F., Antonietti, M., Müller, J. O., Schlögl, R., & Carlsson, J. M. (2008). Graphitic carbon nitride materials: Variation of structure and morphology and their use as metal-free catalysts. *Journal of Materials Chemistry*, 18, 4893–4908. https://doi.org/10.1039/b800274f

Tobaldi, D. M., Pullar, R. C., Gualtieri, A. F., Seabra, M. P., & Labrincha, J. A. (2013). Sol–gel synthesis, characterisation and photocatalytic activity of pure, W-, Ag- and W/Ag co-doped TiO2 nanopowders. *Chemical Engineering Journal*, 214, 364–375. https://doi.org/10.1016/j.cej.2012.11.018

Tsang, C. H. A., Li, K., Zeng, Y., Zhao, W., Zhang, T., Zhan, Y., Xie, R., Leung, D. Y. C., & Huang, H. (2019). Titanium oxide based photocatalytic materials development and their role of in the air pollutants degradation: Overview and forecast. *Environment International*, 125, 200–228. https://doi.org/10.1016/j.envint.2019.01.015

Varma, K. S., Tayade, R. J., Shah, K. J., Joshi, P. A., Shukla, A. D., & Gandhi, V. G. (2020). Photocatalytic degradation of pharmaceutical and pesticide compounds (PPCs) using doped TiO2 nanomaterials: A review. *Water-Energy Nexus*, 3, 46–61. https://doi.org/10.1016/j.wen.2020.03.008

Voon, S., Ong, W., Tan, L., Yong, S., & Chai, S. (2016). Graphene-based semiconductor materials for photocatalytic applications. In M. Aliofkhazraei, N. Ali, W. I. Milne, C. S. Ozkan, S. Mitura, & J. L. Gervasoni (Eds.), *Graphene Science Handbook: Size-Dependent Properties* (pp. 331–348). CRC Press.

Wang, K., Li, Q., Liu, B., Cheng, B., Ho, W., & Yu, J. (2015). Sulfur-doped g-C3N4 with enhanced photocatalytic CO2-reduction performance. *Applied Catalysis B: Environmental*, 176-177, 44–52. https://doi.org/10.1016/j.apcatb.2015.03.045

Wang, P., Huang, B., Dai, Y., & Whangbo, M. H. (2012). Plasmonic photocatalysts: Harvesting visible light with noble metal nanoparticles. *Physical Chemistry Chemical Physics*, 14, 9813–9825. https://doi.org/10.1039/c2cp40823f

Wang, X. J., Yang, W. Y., Li, F. T., Xue, Y. B., Liu, R. H., & Hao, Y. J. (2013). in situ microwave-assisted synthesis of porous N-TiO2/g-C3N4 heterojunctions with enhanced visible-light photocatalytic properties. *Industrial & Engineering Chemistry Research*, 52, 17140–17150. https://doi.org/10.1021/ie402820v

Wang, X., Liu, G., Chen, Z. G., Li, F., Wang, L., Lu, G. Q., & Cheng, H. M. (2009). Enhanced photocatalytic hydrogen evolution by prolonging the lifetime of carriers in ZnO/CdS heterostructures. *Chemical Communications*, 23, 3452–3454. https://doi.org/10.1039/b904668b

Wang, X., & Liu, M. (2019). Photocatalytic enhancement mechanism of direct Z-scheme heterojunction O-g-C3N4@Fe-TiO2 under visible-light irradiation. *Applications of Surface Science*, 485, 353–360. https://doi.org/10.1016/j.apsusc.2019.04.207

Wang, X., Maeda, K., Chen, X., Takanabe, K., Domen, K., Hou, Y., Fu, X., & Antonietti, M. (2009). Polymer semiconductors for artificial photosynthesis: hydrogen evolution by mesoporous graphitic carbon nitride with visible light. *Journal of the American Chemical Society*, 131, 1680–1681.

Wang, Y., Wang, X., & Antonietti, M. (2012). Polymeric graphitic carbon nitride as a heterogeneous organocatalyst: From photochemistry to multipurpose catalysis to sustainable chemistry. *Angewandte Chemie International Edition*, 51, 68–89. https://doi.org/10.1002/anie.201101182

Wen, J., Li, X., Liu, W., Fang, Y., Xie, J., & Xu, Y. (2015). Photocatalysis fundamentals and surface modification of TiO2 nanomaterials. *Chinese Journal of Catalysis*, 36, 2049–2070. https://doi.org/10.1016/s1872-2067(15)60999-8

Wen, J., Xie, J., Chen, X., & Li, X. (2017). A review on g-C3N4-based photocatalysts. *Applications of Surface Science*, 391, 72–123. https://doi.org/10.1016/j.apsusc.2016.07.030

Wu, F., Li, X., Liu, W., & Zhang, S. (2017). Highly enhanced photocatalytic degradation of methylene blue over the indirect all-solid-state Z-scheme g-C3N4-RGO-TiO2 nanoheterojunctions. *Applications of Surface Science*, 405, 60–70. https://doi.org/10.1016/j.apsusc.2017.01.285

Xiao, L., Liu, T., Zhang, M., Li, Q., & Yang, J. (2019). Interfacial construction of zero-dimensional/one-dimensional g-C3N4 nanoparticles/TiO2 nanotube arrays with Z-scheme heterostructure for improved photoelectrochemical water splitting. *ACS Sustainable Chemistry & Engineering*, 7, 2483–2491. https://doi.org/10.1021/acssuschemeng.8b05392

Xiao, X., Wang, Y., Bo, Q., Xu, X., & Zhang, D. (2020). One-step preparation of sulfur-doped porous g-C3N4 for enhanced visible light photocatalytic performance. *Journal of the Chemical Society, Dalton Transactions*, 49(24), 8041–8050. https://doi.org/10.1039/d0dt00299b

Xie, L., Du, T., Wang, J., Ma, Y., Ni, Y., Liu, Z., Zhang, L., Yang, C., & Wang, J. (2021). Recent advances on heterojunction-based photocatalysts for the degradation of persistent organic pollutants. *Chemical Engineering Journal*, 426, 130617. https://doi.org/10.1016/j.cej.2021.130617

Xu, B., Ahmed, M. B., Zhou, J. L., Altaee, A., Xu, G., & Wu, M. (2018). Graphitic carbon nitride based nanocomposites for the photocatalysis of organic contaminants under visible irradiation: Progress, limitations and future directions. *The Science of the Total Environment*, 633, 546–559. https://doi.org/10.1016/j.scitotenv.2018.03.206

Xu, J., Dong, Z., Hu, T., Peng, Y., Situ, Y., & Huang, H. (2019). Construction of TiO2-Fe-C3N4 compound: Promotion of interfacial charge transfer effect through facile energy level alignment. *Journal of Alloys and Compounds*, 781, 140–148. https://doi.org/10.1016/j.jallcom.2018.11.409

Xu, Q., Zhang, L., Yu, J., Wageh, S., Al-Ghamdi, A. A., & Jaroniec, M. (2018). Direct Z-scheme photocatalysts: Principles, synthesis, and applications. *Materials Today*, 21, 1042–1063. https://doi.org/10.1016/j.mattod.2018.04.008

Yadav, S., & Jaiswar, G. (2017). Review on undoped/doped TiO2 nanomaterial; synthes and photocatalytic and antimicrobial activity. *Journal of the Chinese Chemical Society*, 64, 103–116. https://doi.org/10.1002/jccs.201600735

Yahya, N., Aziz, F., Jamaludin, N. A., A. Mutalib, M., Ismail, A. F., W. Salleh, W. N., Jaafar, J., Yusof, N. A., & Ludin, N. (2018). A review of integrated photocatalyst adsorbents for wastewater treatment. *Journal of Environmental Chemical Engineering*, 6, 7411–7425. https://doi.org/10.1016/j.jece.2018.06.051

Yang, L., Bai, X., Shi, J., Du, X., Xu, L., & Jin, P. (2019). Quasi-full-visible-light absorption by D35-TiO2/g-C3N4 for synergistic persulfate activation towards efficient photodegradation of micropollutants. *Applied Catalysis B: Environmental*, 256, 117759. https://doi.org/10.1016/j.apcatb.2019.117759

Yao, Y., Cai, Y., Lu, F., Wei, F., Wang, X., & Wang, S. (2014). Magnetic recoverable MnFe2O4 and MnFe2O4-graphene hybrid as heterogeneous catalysts of

peroxymonosulfate activation for efficient degradation of aqueous organic pollutants. *Journal of Hazardous Materials*, 270, 61–70. https://doi.org/10.1016/j.jhazmat.2014.01.027

Ye, S., Wang, R., Wu, M. Z., & Yuan, Y. P. (2015). A review on g-C3N4 for photocatalytic water splitting and CO2 reduction. *Applications of Surface Science*, 358, 15–27. https://doi.org/10.1016/j.apsusc.2015.08.173

Younis, S., & Kim, K. H. (2020). Heterogeneous photocatalysis scalability for environmental remediation: Opportunities and challenges. *Catalysts*, 10, 1109. https://doi.org/10.3390/catal10101109

Yu, J., Wang, S., Low, J., & Xiao, W. (2013). Enhanced photocatalytic performance of direct Z-scheme g-C3N4–TiO2 photocatalysts for the decomposition of formaldehyde in air. *Physical Chemistry Chemical Physics*, 15, 16883. https://doi.org/10.1039/c3cp53131g

Zhang, J., Zhou, P., Liu, J., & Yu, J. (2014). New understanding of the difference of photocatalytic activity among anatase, rutile and brookite TiO2. *Physical Chemistry Chemical Physics*, 16, 20382–20386. https://doi.org/10.1039/c4cp02201g

Zhang, J. J., Fang, S. S., Mei, J. Y., Zheng, G. P., Zheng, X. C., & Guan, X. X. (2018). High-efficiency removal of rhodamine B dye in water using g-C3N4 and TiO2 co-hybridized 3D graphene aerogel composites. *Separation and Purification Technology*, 194, 96–103. https://doi.org/10.1016/j.seppur.2017.11.035

Zhang, L., Ni, C., Jiu, H., Xie, C., Yan, J., & Qi, G. (2017). One-pot synthesis of Ag-TiO 2 /reduced graphene oxide nanocomposite for high performance of adsorption and photocatalysis. *Ceramics International*, 43, 5450–5456. https://doi.org/10.1016/j.ceramint.2017.01.041

Zhang, S., Gu, P., Ma, R., Luo, C., Wen, T., Zhao, G., Cheng, W., & Wang, X. (2019). Recent developments in fabrication and structure regulation of visible-light-driven g-C3N4-based photocatalysts towards water purification: A critical review. *Catalysis Today*, 335, 65–77. https://doi.org/10.1016/j.cattod.2018.09.013

Zhang, W., Mohamed, A. R., & Ong, W. (2020). Z-Scheme photocatalytic systems for carbon dioxide reduction: Where are we now? *Angewandte Chemie International Edition*, 59, 22894–22915. https://doi.org/10.1002/anie.201914925

Zhang, X., Li, L., Zeng, Y., Liu, F., Yuan, J., Li, X., Yu, Y., Zhu, X., Xiong, Z., Yu, H., & Xie, Y. (2019). TiO2/graphitic carbon nitride nanosheets for the photocatalytic degradation of Rhodamine B under simulated sunlight. *ACS Applied Nano Materials*, 2, 7255–7265. https://doi.org/10.1021/acsanm.9b01739

Zhao, L., Xu, H., Jiang, B., & Huang, Y. (2017). Synergetic photocatalytic nanostructures based on Au/TiO$_2$/reduced graphene oxide for efficient degradation of organic pollutants. *Particle and Particle Systems Characterization*, 34, 1600323. https://doi.org/10.1002/ppsc.201600323

Zhao, W., Yang, X., Liu, C., Qian, X., Wen, Y., Yang, Q., Sun, T., Chang, W., Liu, X., & Chen, Z. (2020). Facile construction of all-solid-state Z-scheme G-C3N4/TiO2 thin film for the efficient visible-light degradation of organic pollutant. *Nanomaterials*, 10(4), 600. https://doi.org/10.3390/nano10040600

Zhou, D., Chen, Z., Yang, Q., Dong, X., Zhang, J., & Qin, L. (2016). In-situ construction of all-solid-state Z-scheme g-C3N4/TiO2 nanotube arrays photocatalyst with enhanced visible-light-induced properties. *Solar Energy Materials and Solar Cells*, 157, 399–405. https://doi.org/10.1016/j.solmat.2016.07.007

Zhou, D., Chen, Z., Yang, Q., Shen, C., Tang, G., Zhao, S., Zhang, J., Chen, D., Wei, Q., & Dong, X. (2016). Facile construction of g-C$_3$N$_4$ nanosheets/TiO$_2$ nanotube arrays as Z-scheme photocatalyst with enhanced visible-light performance. *ChemCatChem*, 8, 3064–3073. https://doi.org/10.1002/cctc.201600828

Zhou, D., Yu, B., Chen, Q., Shi, H., Zhang, Y., Li, D., Yang, X., Zhao, W., Liu, C., Wei, G., & Chen, Z. (2020). Improved visible light photocatalytic activity on Z-scheme g-C3N4 decorated TiO2 nanotube arrays by a simple impregnation method. *Materials Research Bulletin*, 124, 110757. https://doi.org/10.1016/j.materresbull.2019.110757

Zhou, L., Wang, L., Zhang, J., Lei, J., & Liu, Y. (2017). The preparation, and applications of g-C3N4/TiO2 heterojunction catalysts—A review. *Research on Chemical Intermediates*, 43, 2081–2101. https://doi.org/10.1007/s11164-016-2748-8

Zhou, L., Zhang, H., Sun, H., Liu, S., Tade, M. O., Wang, S., & Jin, W. (2016). Recent advances in non-metal modification of graphitic carbon nitride for photocatalysis: A historic review. *Catalysis Science & Technology*, 6, 7002–7023. https://doi.org/10.1039/c6cy01195k

Zhou, Z., Yuan, S., & Wang, J. (2021). Theoretical progress on direct Z-scheme photocatalysis of two-dimensional heterostructures. *Frontiers in Physics*, 16, 43203. https://doi.org/10.1007/s11467-021-1054-0

Zhu, J., Xiao, P., Li, H., & Carabineiro, S. A. C. (2014). Graphitic carbon nitride: Synthesis, properties, and applications in catalysis. *ACS Applied Materials & Interfaces*, 6, 16449–16465. https://doi.org/10.1021/am502925j